frontiers | Frontiers in Sensors

TYPE Review
PUBLISHED 27 October 2022
DOI 10.3389/fsens.2022.1006749

OPEN ACCESS

EDITED BY
Elisabetta Comini,
University of Brescia, Italy

REVIEWED BY
Niravkumar J. Joshi,
Federal University of ABC, Brazil
Dong-Joo Kim,
Auburn University, United States

*CORRESPONDENCE
Sajjad Hajian,
sajjad.hajian@wmich.edu
Massood Z. Atashbar,
massood.atashbar@wmich.edu

SPECIALTY SECTION
This article was submitted to Sensor Devices,
a section of the journal
Frontiers in Sensors

RECEIVED 29 July 2022
ACCEPTED 05 October 2022
PUBLISHED 27 October 2022

CITATION
Hajian S, Maddipatla D, Narakathu BB and Atashbar MZ (2022), MXene-based flexible sensors: A review.
Front. Sens. 3:1006749.
doi: 10.3389/fsens.2022.1006749

MXene-based flexible sensors: A review

Sajjad Hajian*, Dinesh Maddipatla, Binu B. Narakathu and Massood Z. Atashbar*

College of Engineering and Applied Sciences, Department of Electrical and Computer Engineering, Western Michigan University, Kalamazoo, MI, United States

MXenes are an emerging family of two-dimensional (2D) materials which exhibits unique characteristics such as metal-like thermal and electrical conductivity, huge surface area, biocompatibility, low toxicity, excellent electrochemical performance, remarkable chemical stability, antibacterial activity, and hydrophilicity. Initially, MXene materials were synthesized by selectively etching metal layers from MAX phases, layered transition metal carbides, and carbonitrides with hydrofluoric acid. Multiple novel synthesis methods have since been developed for the creation of MXenes with improved surface chemistries using non-aqueous etchants, molten salts, fluoride salts, and various acid halogens. Due to the promising potential of MXenes, they have emerged as attractive 2D materials with applications in various fields such as energy storage, sensing, and biomedical. This review provides a comprehensive overview of MXenes and discusses the synthesis and properties of MXenes, including the methods of etching, delamination, and modification/functionalization, as well as the electrical properties of MXenes. Following this, the recent advances in the development of various MXene-based sensors are presented. Finally, the challenges and opportunities for future research on the development of MXenes-based sensors are discussed.

KEYWORDS

mxenes, sensors, flexible, nanomaterials, two-dimensional materials

1 Introduction

Two-dimensional (2D) materials are composed of layers of strongly bonded atoms, held together by weak interlayer Van der Waals forces (Xu et al., 2013). 2D materials have attracted increasing research attention due to their unique physical, chemical, and electrical properties, such as high surface-to-volume ratio, inherent flexibility, and

Abbreviations: AChE, Acetylcholinesterase; APTES, (3-Aminopropyl)triethoxysilane; ATP, Adenosine triphosphate; AuNP, Au nanoparticle; BSA, Bovine serum albumin; CEA, Carcinoembryonic antigen; CFM, Carbon fiber membranes; Chit, Chitosan; CNT, Carbon nanotube; GCE, Glassy carbon electrode; GCPE, Graphite composite paste electrode; GO, Graphene oxide; GOx, Glucose oxidase; Hb, Hemoglobin; LO, Lactate oxidase; MB, Methylene blue; naf, Nafion; Ni^{2+}, Nickel cation; PB, Prussian blue; PDA, Polydopamine; PDMS, Polydimethylsiloxane; PtNP, Pt nanoparticle; PU, Polyurethane; PVA, Polyvinyl alcohol; rGO, Reduced graphene oxide; SPE, Screen-printed electrode; Tyr, Tyrosinase.

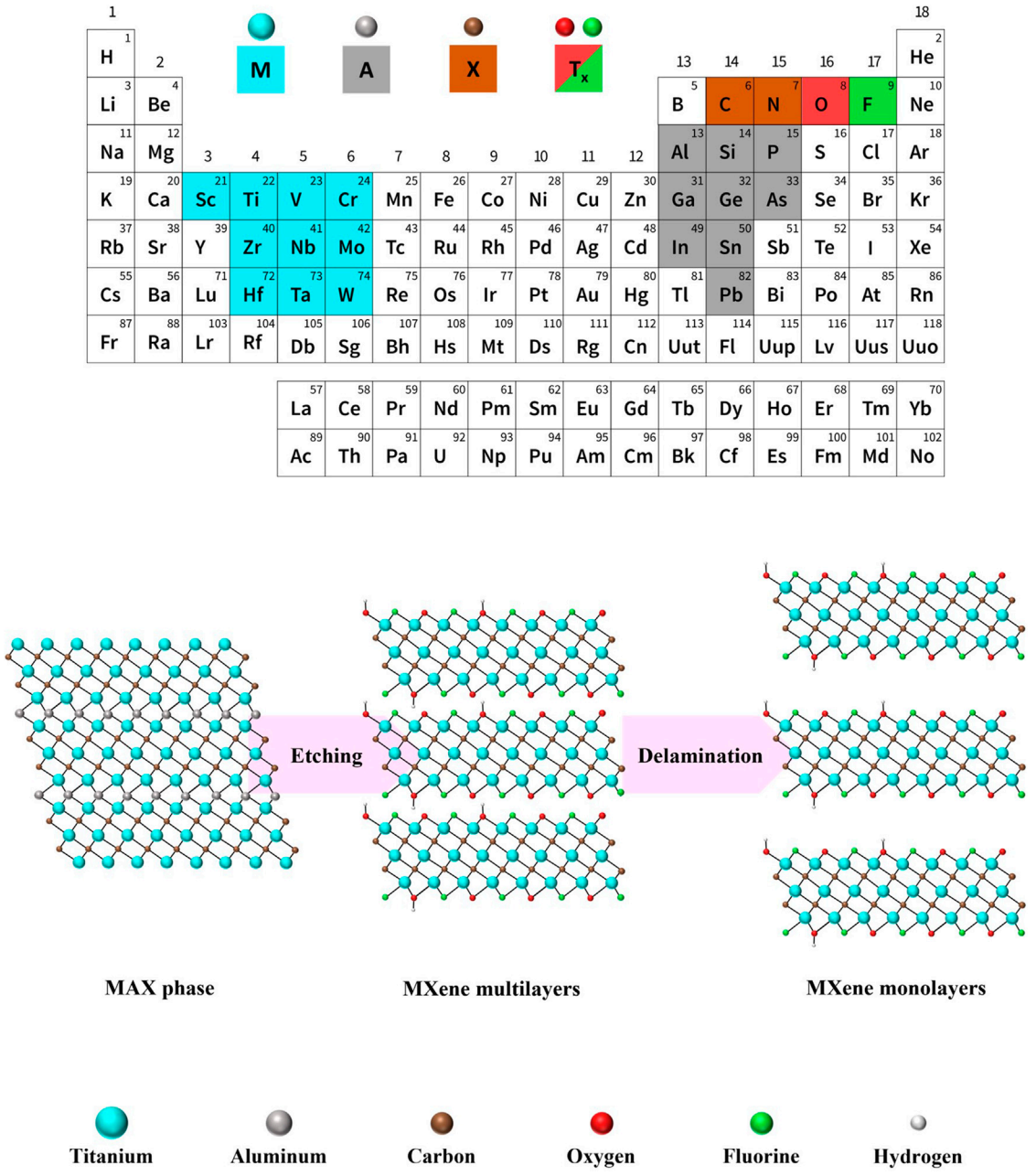

FIGURE 1
(A) A periodic table of elements showing the elements forming MAX phases and MXenes. **(B)** Schematic representation of MXene synthesis through exfoliation process.

modifiable surface properties (Yi et al., 2018; Zhao et al., 2019). These properties have made 2D materials appropriate for various applications, such as energy storage, photonic devices, and sensing applications (Choi et al., 2017).

MXenes, which are transition metal carbides, nitrides, or carbonitrides, are an emerging family of 2D materials, first synthesized by Naguib et al., in 2011 (Naguib et al., 2011). MXenes are synthesized by selective etching of layer A from the layered ternary carbides and nitrides (MAX phase) precursors, which are layered materials formulated as $M_{n+1}AX_n$, where M is an early transition metal (*e.g.*, Sc, Ti, V, Cr, Zr, Nb, Mo, Hf, Ta), A is an element from the group 13 or 14 of the periodic table, and X is carbon and/or nitrogen

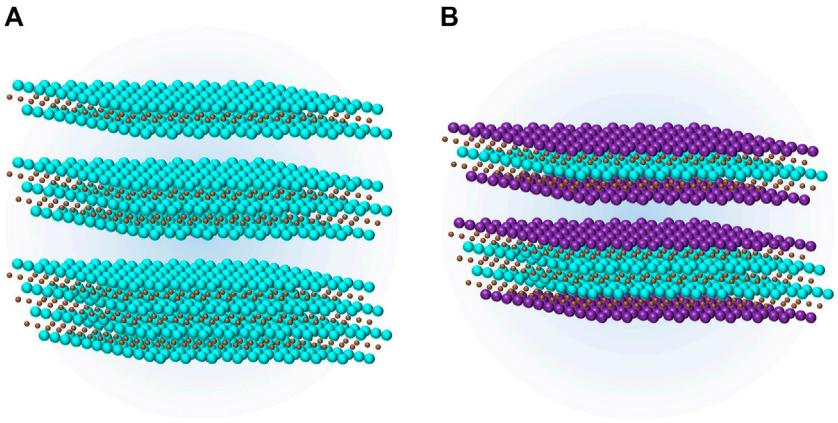

FIGURE 2
(A) The structure of MXenes with different formula: M_2X, M_3X_2, and M_4X_3. **(B)** Two new families of MXenes, ordered double transition metal carbides with $M'_2M''C_2$ and $M'_2M''_2C_3$ formula. M, M′, and M″ are early transition metals and X is carbon and/or nitrogen.

(Figure 1) (Kalambate et al., 2019). The resulting MXenes have the general formula of $M_{n+1}X_nT_x$, where n is an integer from 1 to 3, and T refers to surface functional groups (–OH, –O, and–F). Depending on the application, surface functional groups can be removed by alkalization and calcination treatments (Anasori et al., 2017). MXenes have 2D layered structures, where each X layer is sandwiched between 2 M layers (Figure 2A). In 2015, two new families of MXenes, ordered double transition metal carbides, were predicted and synthesized, increasing the tunability of the MXene family (Figure 2B) (Anasori et al., 2015). These MXene families are formulated as $M'_2M''C_2$ and $M'_2M''_2C_3$, where M′ and M″ are two different early transition metals.

Flexible sensors have attracted significant research interest over the last several decades and have been utilized for developing biomedical devices, wearable devices, and soft robots (Wen et al., 2020). Carbon nanomaterials and 2D materials have been used for developing sensors with improved sensitivity and low power consumption due to their high surface-to-volume ratio, high ion transport properties, inherent flexibility, and modifiable surface properties (Choi et al., 2017). However, the incorporation of these materials in sensor development is limited by undesirable properties such as hydrophobicity, low biocompatibility, low electrical conductivity, and difficulty in surface functionalization (Khan and Andreescu, 2020). However, MXenes provide advantages for the fabrication of high-performance sensors due to their high metallic conductivities up to 24,000 S/cm (Zhang et al., 2017), high hydrophilicity, biocompatibility, ease of surface

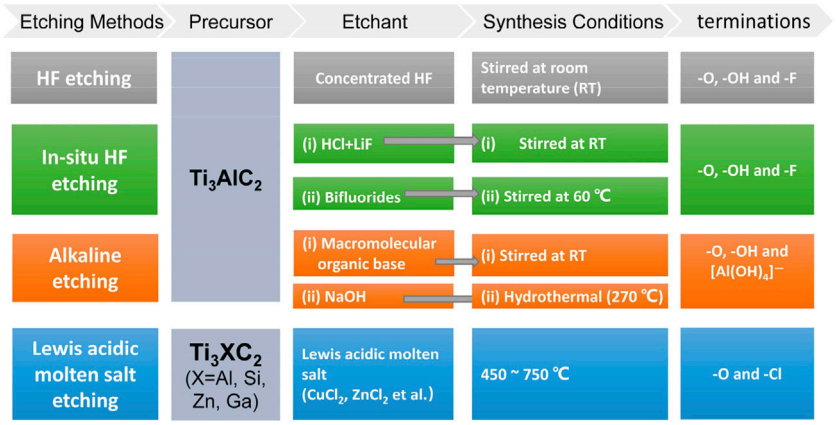

FIGURE 3
Different approaches for the synthesis of titanium carbide MXene ($Ti_3C_2T_x$), Reproduced with permission from Huang et al. (2020), ©American Chemical Society.

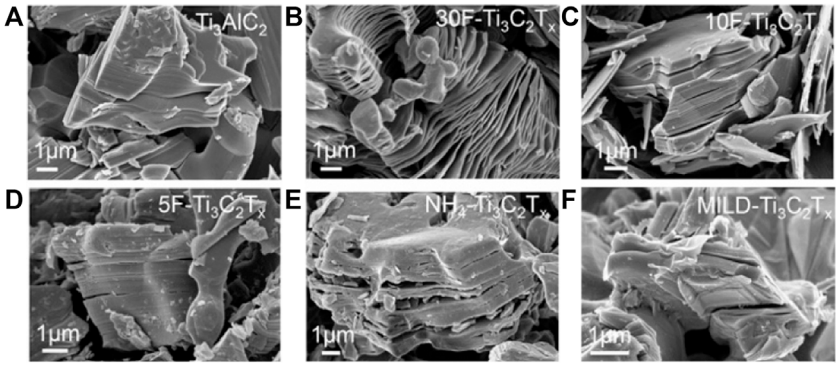

FIGURE 4
SEM image of **(A)** Ti_3AlC_2 (MAX) powder showing the compact layered structure. Multilayered $Ti_3C_2T_x$ powder synthesized with **(B)** 30 wt%, **(C)** 10 wt%, and **(D)** 5 wt% HF. Accordion-like morphology only observed for the 30 wt% HF etched powder **(B)**. **(E)** Multilayered NH_4-$Ti_3C_2T_x$ powder synthesized with ammonium hydrogen fluoride and **(F)** MILD-$Ti_3C_2T_x$ powder etched with 10 M LiF in 9 M HCl, both showing negligible opening of MXene lamellas, similar to what is observed in 5F-$Ti_3C_2T_x$, Reproduced with permission from Alhabeb et al. (2017), ©American Chemical Society.

functionalization, low diffusion barrier, and good intercalation properties (Zhu J. et al., 2017; Hart et al., 2019), which distinguish them from most 2D materials. These advantages have attracted significant research interest in MXenes since 2015, and more than 3,000 MXenes-related articles have been published during the last decade (Carey and Barsoum, 2021; Firouzjaei et al., 2022).

To date, some research and review articles published on MXenes have shown the potential of this material for the development of sensors and electronic devices (Jun et al., 2018; Sinha et al., 2018; Kim et al., 2019; Rasool et al., 2019). However, a comprehensive review of recent progress in the development of MXene-based flexible sensors is missing. This review discusses recent advances in flexible MXene-based sensors (strain, pressure, gas, electrochemical, and optical sensors) and provides detailed discussions on sensing mechanisms and related MXene properties that make MXene a great candidate for sensing applications, as well as challenges and future outlooks. The review initially discusses the synthesis methods of MXenes, including methods of etching, delamination, and modification/functionalization, as well as the electronic structure of MXene. Following this, recent progress in the fabrication of MXene-based chemical, physical, and flexible optical sensors is presented. Finally, the challenges and opportunities for future research on the development of MXenes-based flexible sensors are discussed.

2 Synthesis and electronic structures of MXenes

2.1 Synthesis of MXenes

Various methods have been used to synthesize MXene materials (Figure 3) (Huang et al., 2020). Typically, the synthesis of MXenes includes the etching process to obtain MX phase materials from MAX phase precursors and the delamination process to isolate monolayer MXene flakes. The first report on the synthesis of MXenes included wet-chemical etching with hydrofluoric acid (HF) and resulted in multilayered MXene flakes (Naguib et al., 2011). Using wet-chemical etching with HF, different multilayered MXene compositions were synthesized, such as Ti_2CT_x, Ti_3CNT_x, Nb_2CT_x, and V_2CT_x (Wang et al., 2016). In 2013, monolayer MXene flakes were synthesized by utilizing large organic molecules as intercalants (Mashtalir et al., 2013a). Since the delamination process plays a significant role in the synthesis of monolayer MXene flakes, increasing the delamination yield is of high importance. In 2015, increasing the delamination yield was investigated using organic intercalants such as isopropylamine and tetrabutylammonium hydroxide (TBAOH) (Mashtalir et al., 2015; Naguib et al., 2015). Most of the works reported on the synthesis of MXenes include using MAX phases containing aluminum. In 2018, the most common MAX phase, titanium silicon carbide, was used for large-scale synthesis of titanium carbide MXene (Alhabeb et al., 2018). The obtained delaminated Ti_3SiC_2-derived MXene samples were processed into flexible and conductive films (200 S/cm) with higher oxidation resistance when compared to Ti_3AlC_2-derived MXene. The methods and conditions used in the synthesis process impact the properties of the resulting MXene samples and their performance in the associated applications. In the following, we will discuss the two main processes for the synthesis of MXenes: etching and delamination.

Etching process. Other layered materials, such as graphite and transition metal dichalcogenides (TMDs), have weak van der Waals interactions between their layers, and their

exfoliation process is well studied. In contrast, MAX phases are held together by strong van der Walls interaction, and their exfoliation is more complicated (Ng et al., 2017). So far, different etching methods are used for the development of MXenes, which has led to different synthesis times, defect densities, and surface properties of MXenes (Hope et al., 2016; Hu et al., 2019). As mentioned before, the first etchant used to remove the A layer was hydrofluoric acid (HF). The concentration of HF can influence the synthesis time and properties of the MXene (Hu et al., 2019). Higher HF content decreases the time needed for the etching process, but it introduces more defects to the MXene flakes. According to literature, 2 h is enough for the etching process of Ti_3AlC_2 with ~50 wt% HF at room temperature (Mashtalir et al., 2013b). The effect of using different HF contents (30 wt%, 10 wt%, and 5 wt% HF) for the etching process has been investigated (Alhabeb et al., 2017). It was observed that the 10 wt% and 5 wt% HF etchants did not result in an accordion-like morphology for the MXene, while 30 wt% HF led to MXene samples with an accordion-like structure (Figure 4). Also, it was found that HF content as low as 3 wt% can be used to synthesize $Ti_3C_2T_x$ MXene.

Using HF for the MXene synthesis requires the handling of concentrated HF and a laborious multi-step procedure (Ghidiu et al., 2014). Some alternative MXene synthesis methods were used for *in-situ* HF formation in the etching process, which provides a less hazardous process when compared to using HF acid. As shown in Figure 4, the samples prepared by *in-situ* HF formation have multilayered structures and a negligible opening between MXene layers, which is similar to samples etched by low-concentration HF (Alhabeb et al., 2017). In 2014, Halim et al. used ammonium bifluoride (NH_4HF_2) salt to produce transparent $Ti_3C_2T_x$ MXene films with metallic conductivity (Halim et al., 2014). As another alternative to HF, a mix of lithium fluoride (LiF) salt and hydrochloric acid (HCl) were used as the etchant for the MXene synthesis, which simplified the synthesis of the titanium carbide 'clay' MXene and resulted in films with high volumetric capacitances (Ghidiu et al., 2014). The chemical etchant used in the synthesis process will also influence the surface properties of the prepared MXene samples. Using different etchants will lead to different ratios of surface functional groups resulting in different surface behavior and adsorption kinetics. Hope et al. reported that MXene samples prepared using 50 wt% HF contain nearly four times higher -F surface functional groups compared to MXene samples obtained by HCl-LiF etchant (Hope et al., 2016).

Also, HF-free MXene synthesis methods have been developed, which are less hazardous compared to using HF acid and can result in MXene samples with different surface functional groups and electronic properties. In 2016, an HF-free method was used to synthesize MXene with aluminum oxoanions ($Al(OH)_4^-$) surface groups, showing superior photothermal therapeutic behavior (Xuan et al., 2016). Urbankowski et al. developed a new method using LiF, Sodium fluoride (NaF), and potassium fluoride (KF) molten salts to synthesize titanium nitride MXene ($Ti_4N_3T_x$) (Urbankowski et al., 2016). Li et al. reported a new MXene synthesis method, which is fluoride-free and provides MXenes with exclusively chlorine (Cl) terminations (Li M. et al., 2019). This method included replacing the Al from MAX phases with Zn from molten Zinc chloride ($ZnCl_2$) to form Zn-containing MAX phases. The resulting MAX phases were then exfoliated in the presence of an excess of $ZnCl_2$ to obtain Cl-terminated MXenes. This synthesis method paved the way for producing MXenes with new terminations and surface properties for applications in sensors and other electronic devices. Another fluoride-free method, reported by Yang et al. (2018), included anodic corrosion of Ti_3AlC_2 MAX phases in a binary aqueous electrolyte, resulting in large-scale $Ti_3C_2T_x$ production with a high yield (90%).

Delamination. Generally, the samples resulting from the etching process have a multilayered structure, and a delamination step is necessary to obtain monolayer MXenes. The most common method of delamination is using large organic molecules as intercalants to weaken the interlayer interactions and increase the distance between MXene layers (Lv et al., 2018; Han et al., 2019). Generally, the intercalation and delamination processes include adding a mixture containing intercalants to the multilayered MXene, and a centrifugation process to isolate the delaminated material from the remaining multilayered MXene flakes. Depending on the etching method and the intercalant used, a sonication step might be required to complete the intercalation and delamination process. After the centrifugation process, the colloidal solution of functionalized MXene monolayers can be collected. The flake size, defects, and concentration of the resulted MXene monolayers depend on the sonication process (Malaki et al., 2019). Increasing the sonication power and time will lead to smaller flakes with more defects and may change the MXene sample's concentration. The dispersed MXene nanosheets concentration also depends on other parameters, such as the etchant and intercalants used (Halim et al., 2016).

Alhabeb et al. investigated using different concentrations of LiF/HCl mixtures as the etchant (Alhabeb et al., 2017). It was observed that there was no need to add intercalants when using Lif/HCl etchant, and the necessity of using a sonication step for delamination depends on the concentrations of LiF and HCl. The delamination process for multilayered $Ti_3C_2T_x$ MXene produced by 5 M LiF/6 M HCl etchant requires sonication, resulting in small MXene flakes with high defects. However, for the MXene synthesis method using 7.5 M LiF/9 M HCl, the delamination process can be done by hand-shaking of samples, resulting in large monolayer MXene flakes with fewer defects. This increases its electrical conductivity, but choosing the suitable flake size and defect density depends on the application of the MXene-based device.

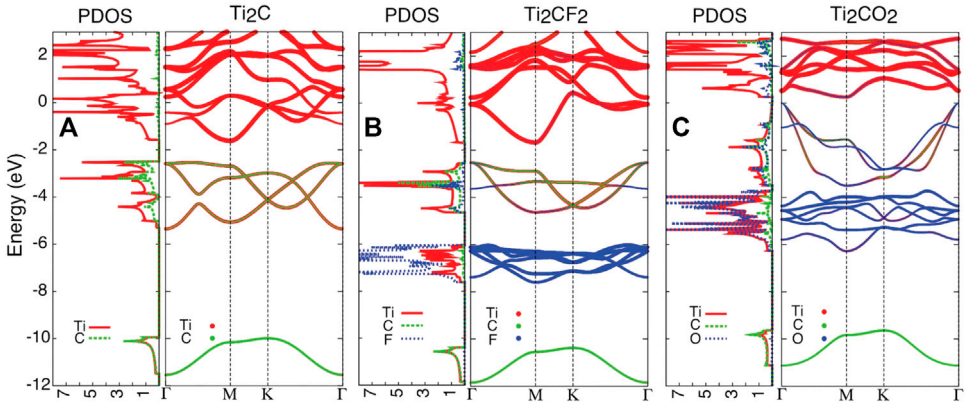

FIGURE 5
Projected density of states [PDOS (states per eV per cell)] and projected band structures for **(A)** Ti_2C, **(B)** Ti_2CF_2, and **(C)** Ti_2CO_2. The Fermi energy is located at zero energy, Reproduced with permission from Khazaei et al. (2017), ©Royal Society of Chemistry.

2.2 Electronic structures of MXenes

The electronic structure of the obtained MXene samples depend on the M and X elements, as well as surface functional groups. During the MXene synthesis process, surface terminations will replace A layers of the MAX phases, such that the surfaces of the resulting MXene layers are functionalized, usually with -F, -O, or -OH functional groups. As discussed before, different MXene synthesis methods will lead to different properties such as flake size, defect density, and surface functional groups, which in turn affect their electronic structure. MXenes can have metallic or semiconductor-like behavior. Two outer transition metal layers have a significant effect on the electronic structure, and the metallic or semiconductor-like behavior of the MXene can be controlled by changing these two layers (Anasori et al., 2016). For example, some ordered double transition metal carbides, such as molybdenum titanium carbide ($Mo_2TiC_2T_x$), have semiconductor-like behavior (Anasori et al., 2016). Also, changing surface functional groups and intercalant molecules can lead to transitions between metallic and semiconductor-like behavior (Hart et al., 2019).

In most MXenes, there is a small band gap between the *p* bands of C/N atoms and the d bands of the early transition metal (Figure 5) (Khazaei et al., 2017). Upon functionalization of MXenes, the hybridization between d orbitals of transition metal and *p* orbitals of terminating groups will generate new bands below the Fermi energy (Khazaei et al., 2019). Also, as transition metals have lower electronegativity than C/N atoms and the surface functional groups, the transition metal atoms become positively charged by donating electrons to C/N atoms and surface functional groups (Khazaei et al., 2013). The surface functional groups with different electronegativity influence the electrical and ion transport properties of MXenes, which impact their conductivity and charge transfer to their surfaces (Khazaei et al., 2017). Some of the OH-terminated MXenes, such as $Sc_2C(OH)_2$ and $Hf_2C(OH)_2$, have partially occupied nearly free electron (NFE) states. These NFE states are close to the Fermi energy since the OH-terminated MXenes have positively charged hydrogen atoms at their surfaces. NFE states can provide almost perfect transmission channels without nuclear scattering for electron transport.

As discussed, the band structure and band gap of MXenes can be controlled by changing many parameters, which makes them promising materials for sensing applications. MXenes have been used for the detection of several gases and molecules due to the conductivity changes upon the adsorption of target species on the MXenes (Huang et al., 2018). Interactions of these molecules with the MXene's surface lead to the change of terminations, which in turn changes the conductivity of MXenes. Also, the band gap of Ti_2CO_2 and Sc_2CO_2 MXenes experiences a considerable change by applying strain or an external electric field (Khazaei et al., 2017).

3 MXenes as sensors

Although MXenes emerged less than a decade ago, they have attracted significant attention as potential materials for the fabrication of high-performance sensors due to their multiple unique properties. In this section, the application of MXenes for the fabrication of physical, chemical, and optical sensors is discussed.

3.1 Physical sensors

Physical sensors convert a physical quantity, such as force or temperature, into electrical signals. Pressure sensors, strain

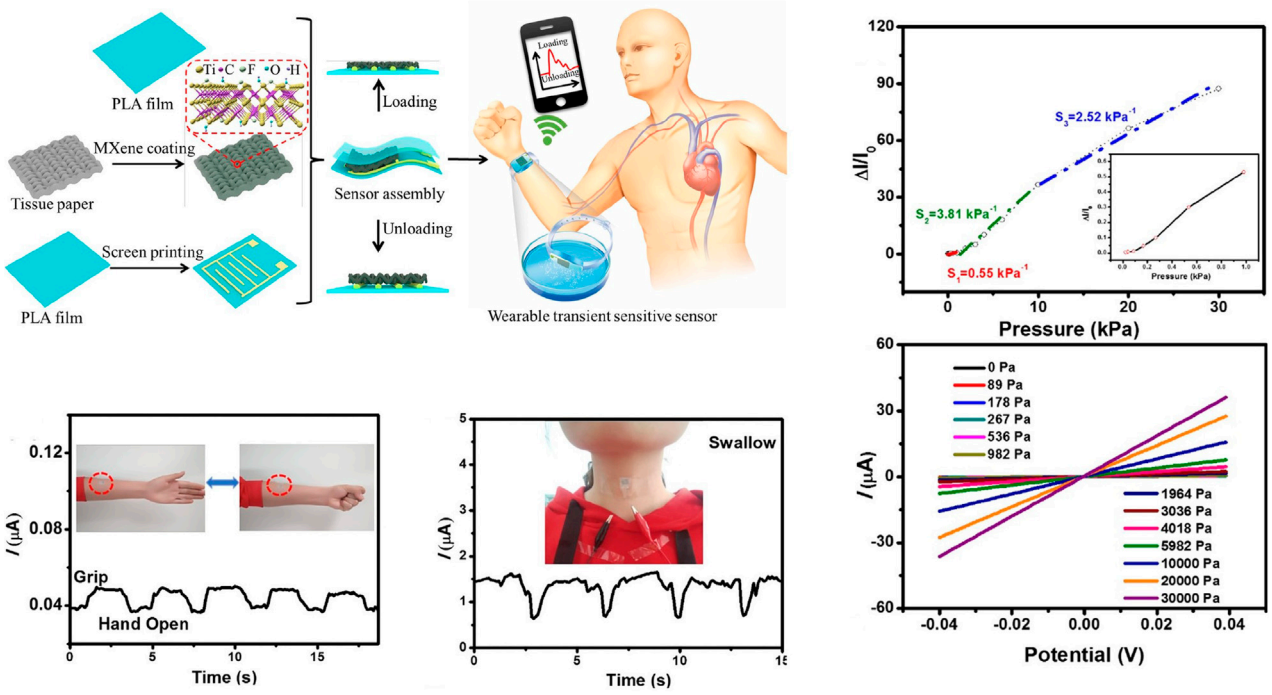

FIGURE 6
(A) Schematic illustration of the fabrication procedure of flexible wearable transient pressure sensors with MXene nanosheets. **(B)** Sensing performance of the pressure sensor attached to the arm muscle for reliable detection of radial muscle contraction resulting from reversibly making a fist. Inset: Photograph of the sensor attached onto the arm muscle while reversibly making a fist. **(C)** Sensing performance of the pressure sensor adhered onto a human throat for the timely sensing of swallowing. Inset: Photograph of the sensor attached onto a human throat. **(D)** Sensing sensitivity of the flexible pressure sensor to pressure. **(E)** I–V curves of the sensor with various applied pressures, Reproduced with permission from Guo et al. (2019), ©American Chemical Society.

sensors, and temperature sensors are some examples of physical sensors. Among these sensor types, MXenes have been used extensively for the development of pressure sensors and strain sensors. Therefore, this review focuses on pressure sensors and strain sensors.

3.1.1 Pressure sensors

Pressure sensors are utilized in various applications such as human motion monitoring, tactile sensing, and artificial intelligence (Zang et al., 2015). There are different pressure sensing mechanisms, including piezoresistive sensing, capacitive sensing, and piezoelectrical sensing. In piezoresistive sensors, the applied pressure causes a change in the resistance of the sensor. In a capacitive sensing mechanism, an applied pressure deflects the capacitor's plates, leading to a change in the capacitance. Piezoelectric-based sensors are based on certain types of solid materials which generate electrical charges in response to applied pressure. The rapid growth of novel nanomaterials and fabrication techniques has enabled the development of flexible pressure sensors with improved properties, such as high flexibility, low cost, and compatibility with large-area production. MXenes can be used for the fabrication of flexible pressure sensors since the distances and interactions between MXene layers can be changed under an external force which changes the electrical resistance, (Wu et al., 2021). However, there are challenges faced by MXene-based composites, such as the low mechanical strength and elasticity of MXene-based aerogel pressure sensors, which can be overcome by creating long-range ordered structures using bidirectional freezing or other technologies. In addition, the low sensitivity of MXene-based fabric pressure sensors can be resolved by chemical cross-linking or using cross-linking agents as bridges (Wu et al., 2021). Ma et al. investigated the pressure-sensing capabilities of MXene/reduced graphene oxide (MX/rGO) nanocomposite, which combines the large specific surface area of rGO and the high conductivity of MXene ($Ti_3C_2T_x$) (Ma et al., 2018). The porous structure of the synthesized MX/rGO nanocomposite led to superior pressure sensing performance compared to that of rGO or MXene. It was reported that the MXene flakes would be wrapped with large rGO nanosheets inside the aerogel, which can prevent the poor oxidization of MXene. The obtained light and elastic MX/rGO-based aerogels were used to fabricate piezoresistive

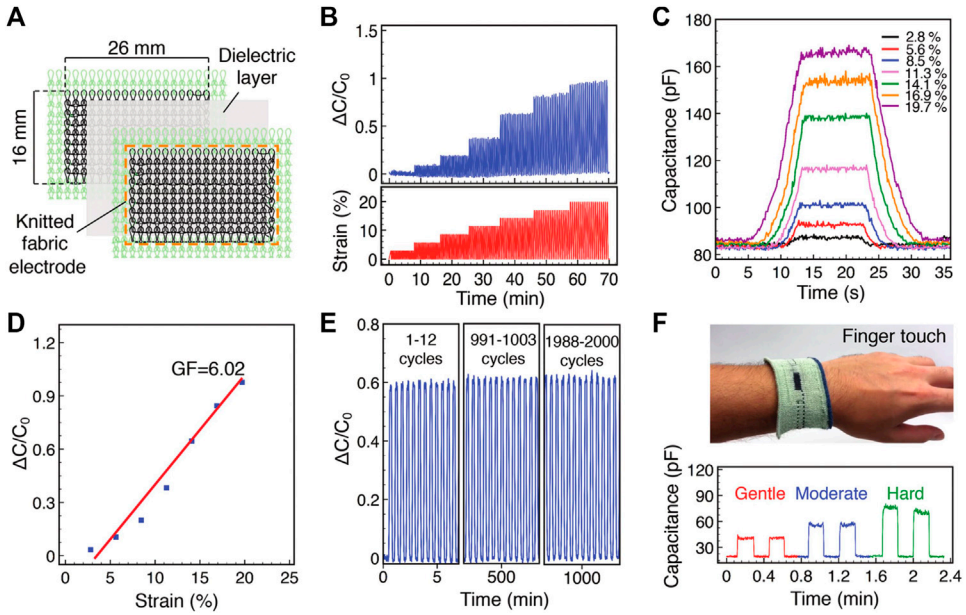

FIGURE 7
Evaluation of sensing performance of the capacitive knitted pressure sensor device. **(A)** Schematic representation of the capacitive pressure sensor (active area—16 mm × 26 mm) assembled by using two knitted fabric electrodes and a dielectric layer. **(B)** Electromechanical behavior of the knitted sensor. The applied strain is incrementally increased from 2.8 to 19.7%. Each cyclic deformation is repeated 20 times. **(C)** Capacitance as a function of time at different compression strains ranging from 2.8 to 19.7%. The hold time is 10 s. **(D)** Relative capacitance changes of the sensor at various strains. Gauge factor (GF) is derived from the linear fit. **(E)** Cyclic stability of the sensor based on relative capacitance change at 14.1% strain for 2000 cycles. **(F)** Top: Photograph of the knitted pressure sensor button (active area—16 mm × 5 mm). Bottom: capacitance output of the sensor when a gentle, moderate, or hard pressure is applied to the device by a finger, Reproduced with permission from Uzun et al. (2019), ©Wiley-VCH.

TABLE 1 Summary of MXene-based pressure sensors.

Sensing material	Sensitivity (kPa-1)	Limit of detection (Pa)	Response time (ms)/Recovery time (ms)	Ref
MXene/rGO aerogel	4.05 for <1 kPa 22.56 for >1 kPa	10	245/212	Ma et al. (2018)
MXene–coated textile	3.844 for <29 kPa 12.095 for 29–40 kPa	-	26/50	Li T. et al. (2019)
MXene-impregnated tissue paper	0.55 for 23–982 Pa 3.81 for 0.982–10 kPa 2.52 for 10–30 kPa	10.2	11/-	Guo et al. (2019)
MXene-sponge/PVA Nanowires	147 for <5.37 kPa 442 for 5.37–18.56 kPa	9	138/-	Yue et al. (2018)
$Ti_3C_2T_x$/natural microcapsule bio-composite	24.63 for 0–0.2 kPa 1.18 for 0.2–7 kPa	8	14/-	Wang et al. (2019)
Carbonized $Ti_3C_2T_x$ aerogel/bacterial cellulose	12.5 for 0–10 kPa	1	167/121	Chen et al. (2019)
MXene/chitosan/PU sponge	0.014 for <6.5 kPa −0.015 for 6.5–85.1 kPa −0.001 for >85.1 kPa	9	19/-	Li X. P. et al. (2019)
Knitted MXene-coated yarn	-	2	-/-	Uzun et al. (2019)

pressure sensors with a 3D structure. The fabricated MX/rGO aerogel-based pressure sensors showed a sensitivity of 22.56 kPa^{-1}, a response time of <200 ms, and good stability over 10,000 cycles, which can detect the pressure below 10 Pa.

Flexible and degradable pressure sensors have potential use in many applications such as electronic skins, flexible displays, and intelligent robotics. Guo et al. developed a flexible and degradable pressure sensor by sandwiching porous MXene-impregnated tissue paper between a biodegradable polylactic acid (PLA) thin sheet and an interdigitated electrode-coated PLA thin sheet (Figure 6) (Guo et al., 2019). The flexible pressure sensor exhibited a detection limit of 10.2 Pa, detection range up to 30 kPa, a response time of 11 ms, low power consumption (10–8 W), good stability over 10,000 cycles, and excellent degradability. The pressure sensors were attached to the arm muscle, cheek, throat, and wrist and showed promising responses for human motion monitoring. Also, E-skin assembled from the MXene/tissue-paper-based sensors with a size of four pixels × 4 pixels was used for pressure mapping. Remote touching monitoring was demonstrated using the wireless connection of the sensor to a mobile phone. Employing biodegradable and biocompatible materials in the fabrication of pressure sensors has the potential to decrease electronic waste, which is one of the fastest-growing pollution problems worldwide contaminating the environment (Heacock et al., 2015).

Textile-based electronics enable the next generation of wearable electronic devices and has recently attracted significant research interest. Uzun et al. developed a fully knitted textile-based capacitive pressure sensor based on MXene-coated cotton yarn (Figure 7) (Uzun et al., 2019). The fabricated sensor exhibited a gauge factor of ≈6.02, a sensing range for up to ≈20% compression, and good stability over 2000 cycles. Integrating MXene in cellulose-based yarns can pave the way for the development of various textile-based electronic devices. Li et al. used MXene–coated textile, prepared by a simple dip-coating process, to develop a flexible piezoresistive pressure sensor (Li T. et al., 2019). The textile was dip-coated in $Ti_3C_2T_x$ MXene, and the MXene-coated textile was sandwiched between two molybdenum (Mo) interdigitated electrodes and polyimide (PI) tape. The fabricated pressure sensors exhibited a sensitivity of 12.095 kPa^{-1} for the 29–40 kPa range and 3.844 kPa^{-1} for the pressures <29 kPa, a response time of 26 ms, and good stability over 5,600 cycles. The obtained conformal MXene–textile sensors demonstrated the potential of being used for monitoring human physiological signals, such as pulses, voice, or finger movements. Further, a 4 × 4 pressure sensor array was fabricated and used for pressure distribution mapping, thereby demonstrating the potential of the MXene-textile pressure sensors as wearable devices for human-machine interface applications.

Recently, a sponge-based piezoresistive pressure sensor was developed by treating the backbone of polyurethane (PU) sponge with chitosan (CS) to obtain positively charged CS/PU sponge, followed by dip-coating of negatively charged $Ti_3C_2T_x$ MXene sheets (Chen et al., 2019). The fabricated sensor exhibited a low detection limit of 30 μN (corresponding to a pressure of 9 Pa), a response time of 19 ms, good stability over 5,000 cycles, and stable piezoresistive response for compressive strains up to 85% with the stress of 245.7 kPa. The sensor also showed a stable performance after washing in water for 1 h. The developed sensor was used for detecting human physiological signals and insect movements, as well as non-contact signals such as voice and human breath. Also, MXene has been used to improve the piezoelectric response of polyvinylidene-fluoride-trifluoroethylene (PVDF-TrFE), which in turn was used to develop self-powered linear pressure sensors (Wang S. et al., 2021). The developed sensors exhibited improved output voltage, depending on the MXene content. The pressure sensor was fabricated by electrospinning PVDF-TrFE/MXene nanofiber mats. MXene has effective interaction with the dipoles of PVDF-TrFE molecular chains and can potentially increase the polarization of PVDF-TrFE during electrospinning due to MXene's large amount of surface functional groups and its high electrical conductivity. The developed sensor exhibited a linear voltage-pressure response. Also, the sensor was capable of harvesting mechanical energy and sensing body motion, which can be used for developing self-powered pressure sensors for healthcare applications. A summary of MXene-based pressure sensors is listed in Table 1.

3.1.2 Strain sensors

The working principle of a strain sensor originates from the resistance change under strain (ε), which is the relative change in length ($\varepsilon = \Delta l/l$). The resistance is given by $R = \rho l/A$, where ρ, l, and A are electrical resistivity, length, and cross-sectional area. The gauge factors (GF), which is the ratio of relative resistance change to strain, is expressed as $1+2\upsilon+\Delta\rho/\varepsilon\rho$, where υ is the Poisson's ratio (Duan et al., 2020). Strain sensors have attracted significant research interest for various applications such as robotics, human motion monitoring, and electronic skin (Ge et al., 2018). It is desired to fabricate strain sensors that have high gauge factors (GF) and work for a broad range of strains. Also, the rapidly growing area of flexible and wearable electronics necessitates the development of flexible and stretchable strain sensors. Desired materials for strain sensing should be able to show large structural changes when a small strain is applied to the sensor. Novel nanocomposites, such as Graphene/PDMS and CNT/PDMS, have been used to develop flexible strain sensors (Yan et al., 2018). Generally, it is challenging to fabricate strain sensors with both high GF (>100) and a broad sensing range (>100%). Recently, MXenes have also been investigated for the fabrication of strain sensors. Due to possible interaction between adjacent layers of MXene, pure MXene structures have limited slippage between the layers under the applied strain and generate cracks to disperse the strain, which may lead to ultra-high

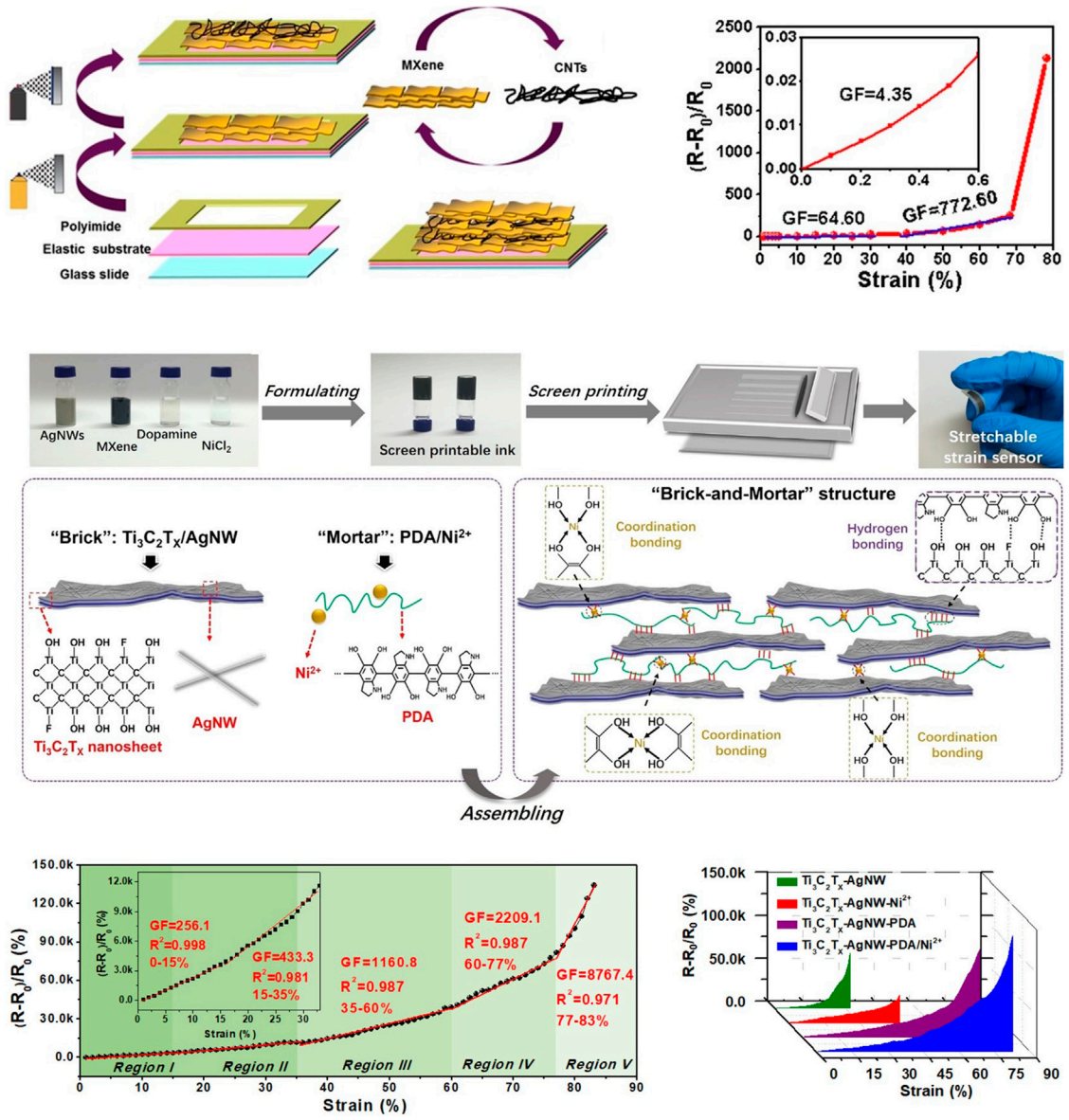

FIGURE 8
(A) Fabrication process of a sandwich-like $Ti_3C_2T_x$ MXene/CNT layer, and typical relative resistance–strain curve of a $Ti_3C_2T_x$ MXene/CNT/latex strain sensor at a stretching rate of 5% min. The inset shows the curve within 0.6% strain, Reproduced with permission from Cai et al. (2018), ©American Chemical Society. **(B)** Schematic of the fabrication process for the bioinspired $Ti_3C_2T_x$-AgNW-PDA/Ni^{2+} sensor fabricated through the screen-printing method. Schematic illustration of the structures for the "brick" materials ($Ti_3C_2T_x$ and AgNWs), "mortar" material (PDA/Ni^{2+}), and the $Ti_3C_2T_x$-AgNW-PDA/Ni^{2+} sensor based on the "brick-and-mortar" architecture is shown. Detailed gauge factor and linear behavior of the $Ti_3C_2T_x$-AgNW-PDA/Ni^{2+} strain sensor is illustrated. Regions I, II, III, IV, and V represent the fitting lines for strains ranging from 0 to 15% (with a linearity of 0.998), 15–35% (with a linearity of 0.981), 35–60% (with a linearity of 0.987), 60–77% (with a linearity of 0.987), and 77–83% (with a linearity of 0.971), respectively (GF = gauge factor). Typical relative resistance change as a function of applied strain curves for the $Ti_3C_2T_x$-AgNW, $Ti_3C_2T_x$-AgNW-PDA, $Ti_3C_2T_x$-AgNW-Ni^{2+}, and $Ti_3C_2T_x$-AgNW-PDA/Ni^{2+} sensors is shown, Reproduced with permission from Shi et al. (2019), ©American Chemical Society.

GF in a small strain range but limits the operating range of the sensor (Zeng and Wu, 2021). To address this problem, MXene/polymer composites have been used to develop strain sensors, where a stretchable polymer absorbs the applied strain and generates the deformation, and conductive MXene layers generate electrical signal changes (Zeng and Wu, 2021).

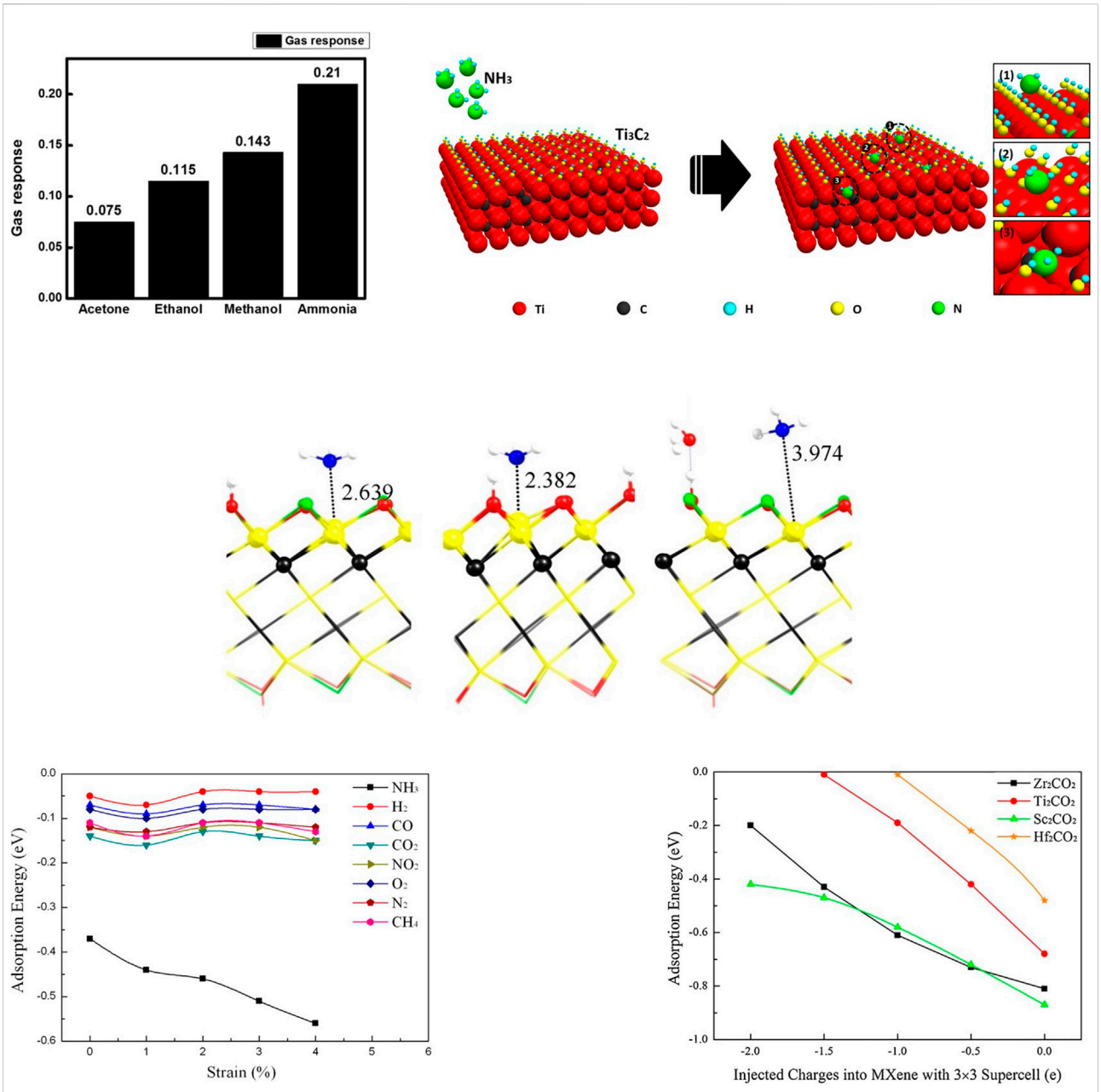

FIGURE 9
(A) Calculated average gas response of the $Ti_3C_2T_x$ MXene-based gas sensor for different gases, and schematic illustration of the possible gas-sensing mechanisms of the $Ti_3C_2T_x$ MXene for NH_3 gas, Reproduced with permission from Lee et al. (2017), ©American Chemical Society. **(B)** Side view of the adsorption structures of the NH_3 gas molecule on the surface of MXenes with different types of surface functional groups. Yellow, black, red, green, white, and blue atoms are titanium, carbon, oxygen, fluorine, hydrogen, and nitrogen, respectively. Binding distances are in Å, Reproduced with permission from Khakbaz et al. (2019), ©American Chemical Society. **(C)** Adsorption energies of gas molecules (including NH_3, H_2, CH_4, CO, CO_2, N_2, NO_2, or O_2) on monolayer Ti_2CO_2 as a function of applied biaxial strains (from 0 to 4%), Reproduced with permission from Yu et al. (2015), ©American Chemical Society. **(D)** The adsorption energies of NH_3 on monolayer Sc_2CO_2, Ti_2CO_2, Zr_2CO_2, and Hf_2CO_2, Reproduced with permission from Xiao et al. (2016), ©Elsevier.

Recently, the development of a highly sensitive strain sensor with a tunable sensing range based on $Ti_3C_2T_x$ MXene/CNT composite has been reported (Figure 8A) (Cai et al., 2018). A soft latex rubber was used as the substrate, and $Ti_3C_2T_x$, as well as CNTs, were alternately deposited into sandwiched $Ti_3C_2T_x$/CNT thin films by air-spray coating.

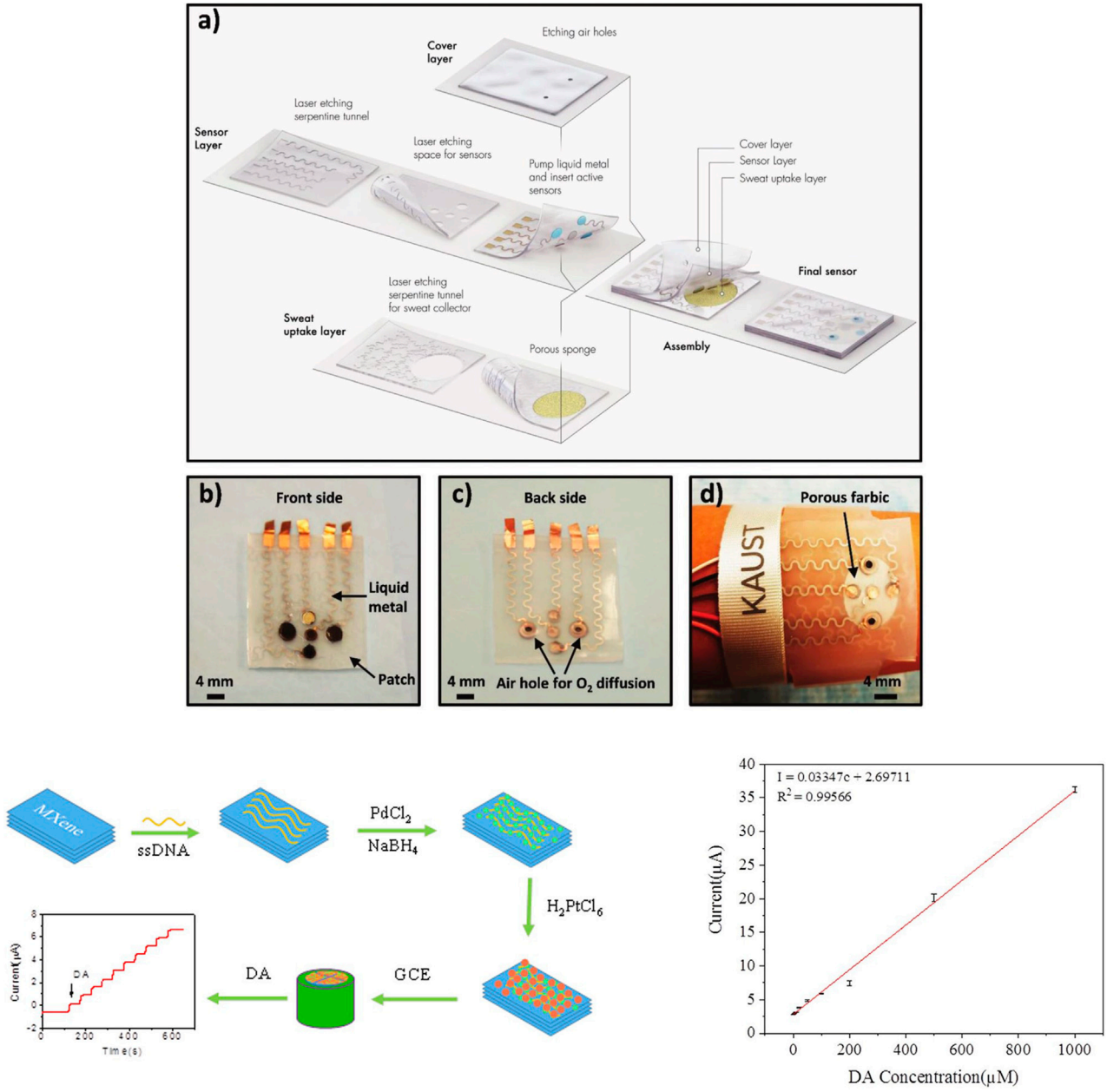

FIGURE 10
(A) Schematic illustration of the stretchable and wearable biosensor based on MXene/Prussian blue (Ti3C2/PB) composite, which is composed of a sweat-uptake layer, a sensor layer, and a cover layer. The optical images show the front-side and back-side of the sensor, as well as the sensor wristband laminated on human skin, Reproduced with permission from Lei et al. (2019), ©Wiley-VCH. **(B)** The schematic diagram of the fabrication of Ti_3C_2/DNA/Pd/Pt nanocomposite, and the linear calibration curve of the response current vs DA concentration for Ti_3C_2/DNA/Pd/Pt/GCE in stirred 0.1 M pH 7.0 PBS containing 0.2–5,000 μM DA. The error bars are standard deviations of three measurements, Reproduced with permission from Zheng et al. (2018a), ©Elsevier.

The MXene/CNT composite combined the sensitive MXene nanosheets with conductive and stretchable CNT crossing. The fabricated strain sensors with thin device dimensions (<2 μm in thickness) were able to detect small deformations (detection limit of 0.1% strain) and large deformations (up to 130% strain). Also, these sensors exhibited stretchability up to 130%, high sensitivity (GF ~ 772.6), tunable maximum strain limit (up to 130% strain), and good durability

TABLE 2 Summary of MXene-based strain sensors.

Sensing material	Gauge factor	Strain range	Ref
MXene nanocomposite organohydrogel	5.02	0–200%	Liao et al. (2019)
	44.85	200–350%	
$Ti_3C_2T_x$/graphene/PDMS	190.8	0–52.6%	Yang Y. et al. (2019a)
	1,148.2	52.6–74.1%	
$Ti_3C_2T_x$/PVA hydrogel	0.40 (Capacitive)	0–200%	Zhang J. et al. (2019)
Sliver nanowire/waterborne PU/MXene	128	0–15%	Pu et al. (2019)
	800	15–25%	
	1,553	25–50%	
	3.2×10^5	50–70%	
	3×10^6	70–85%	
	1.6×10^7	85–100%	
$Ti_3C_2T_x$-based PVA hydrogel	25	0–40%	Zhang et al. (2018)
$Ti_3C_2T_x$ nanoparticle-nanosheet network	178.4	0–5%	Yang Y. et al. (2019b)
	505.1	5–35%	
	1,176.7	35–53%	
$Ti_3C_2T_x$ MXene/CNT	64.6	0–30%	Cai et al. (2018)
	772.6	40–70%	
$Ti_3C_2T_x$ MXene/silver nanowire/PDA/Ni^{2+}	256.1	0–15%	Shi et al. (2019)
	433.3	15–35%	
	1,160.8	35–60%	
	2,209.1	60–77%	
	8,767.4	77–83%	
$Ti_3C_2T_x$ MXene	180.1–94.8	0.19–0.82%	Ma et al. (2017)
	94.8–45.9	0.82–2.13%	
MXene/PU	22.9	0–10%	Yang K. et al. (2019)
	228	10–100%	
$Ti_3C_2T_x$ MXene/PU composite fibers	2.38 at 50% strain	0–152%	Seyedin et al. (2020)
	129 at 152% strain		
Polyimide nanofiber/MXene composite aerogel	-	0.5–16%	Liu et al. (2021)
	1.67	16–60%	
	-	60–90%	

for >5,000 cycles. The fabricated sensors were used for the detection of body motions. Recently, a wearable strain sensor based on an anti-freeze MXene nanocomposite organohydrogel (MNOH) has been developed for extremely low-temperature conditions (Liao et al., 2019). The self-healing and conductive MNOH, synthesized by immersing MXene nanocomposite hydrogel (MNH) in ethylene glycol (EG) solution, maintained flexibility and reversible bending capability at −40°C. The fabricated strain sensors, with a gauge factor of 44.85 under extremely low temperatures (−40°C), were able to measure strain levels up to 350%. The developed wearable strain sensors were used for the detection of human motion, such as finger bending and swallowing. MXenes are also used for the development of capacitive strain sensors. Zhang et al. developed a highly stretchable and self-healing electrode based on MXene ($Ti_3C_2T_x$)/polyvinyl alcohol (PVA) hydrogel (Zhang J. et al., 2019). Adding MXene to PVA increases the conductivity and self-healability of the hydrogel, leading to highly stretchable (≈1,200%) electrodes with a self-healing time of ~0.15 s. The fabricated capacitive strain sensors showed high linearity up to 200% strain, a sensitivity of ≈0.40, and good durability for 10,000 cycles.

Shi et al. developed bio-inspired strain sensors based on a nacre-mimetic microscale "brick-and-mortar" architecture, with 2D titanium carbide (MXene) $Ti_3C_2T_x$/1D silver nanowire as "brick" and polydopamine (PDA)/Ni^{2+} as "mortar" (Figure 8B) (Shi et al., 2019). The sensor demonstrated a gauge factor of >200 over a range of working strains up to 83% and achieved a gauge factor exceeding 8,700 in the strain region of 76–83%. The microscale hierarchical architecture derived from the combination of the "brick" and "mortar" and the

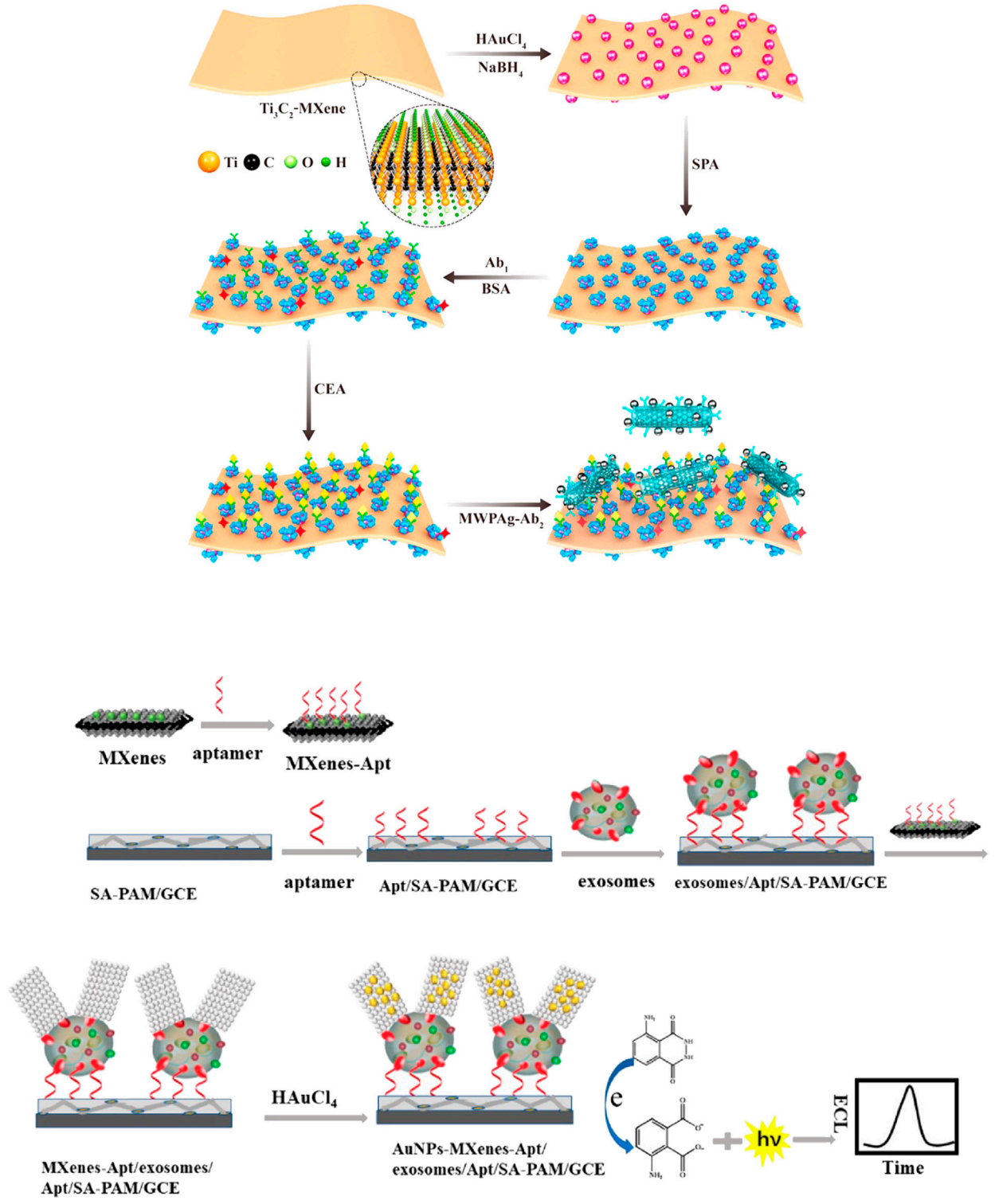

FIGURE 11
(A) Schematic of surface plasmon resonance (SPR) biosensors for detecting CEA, Reproduced with permission from Wu Q. et al. (2019), ©Elsevier. **(B)** Principle of the electrochemiluminescence (ECL) biosensor for detecting exosomes based on *in-situ* formation of AuNPs decorated Ti_3C_2 MXenes nanoprobes, Reproduced with permission from Zhang et al. (2020), ©American Chemical Society.

synergistic toughening effects from interfacial interactions of hydrogen and coordination bonding, layer slippage, and molecular chain stretching can lead to the combination of high sensitivity and large stretchability. The developed sensors were attached to the human wrist and knee and showed successful pulse monitoring and knee bending detection.

Seyedin et al. developed a wearable strain sensor based on $Ti_3C_2T_x$ MXene/polyurethane (PU) composite fibers (Seyedin et al., 2020). A scalable wet-spinning technique was used to produce $Ti_3C_2T_x$ MXene/PU composite conductive fibers with high stretchability. The fabricated strain sensor had a gauge factor of ≈129 (≈2.38 at 50% strain) and a strain range of ≤152%. The knitted MXene/PU fibers were used as wearable strain sensors and showed successful gait detection. This study presented strategies for producing MXene-based fibers to develop wearable electronic devices. Recently, Liu et al. developed a conductive polyimide nanofiber (PINF)/MXene composite aerogel using freeze-drying and thermal imidization process (Liu et al., 2021). The developed composite aerogel exhibited a low density (9.98 mg cm^{-3}), temperature tolerance from −50 to 250°C, improved compressibility and recoverability (up to 90% strain), and fatigue resistance over 1,000 cycles. The composite aerogel was used to develop a strain sensor with a maximum strain limit of 90% (corresponding 85.21 kPa), a detection limit of 0.5% strain (corresponding 0.01 kPa), and good stability over 1,000 cycles. The composite aerogel exhibited a stable piezoresistive sensing ability in harsh environments, such as liquid nitrogen and a high temperature of 150°C. Also, the developed sensor exhibited good performance for the detection of human body motion. A summary of the characteristics and performance of MXene-based strain sensors is listed in Table 2.

3.2 Chemical sensors

Chemical sensors are used to convert a chemical property of an analyte into electrical signals. MXenes are used for the development of chemical sensors, including gas sensors, humidity sensors, and electrochemical sensors, which are discussed in this section. During the synthesis of MXenes, the usage of different etching agents and intercalation agents results in the surface functionalization of MXenes with different functional groups, offering numerous possibilities for surface state engineering (Khan and Andreescu, 2020; Mehdi Aghaei et al., 2021). It is also feasible to tune the number of valence electrons and the relativistic spin-orbit coupling using transition metals in the synthesis (Khazaei et al., 2017). The functionalization of MXenes surface with a particular functional group and tuning of its properties will exhibit affinity towards a certain analyte, and this provides the ability to selectively bind the analyte for specific targeting and recognition, which is essential for sensing. In other words, by changing the surface functional groups of MXenes, the interactions between analytes and the MXene can be controlled, resulting in the selective chemical sensing properties of MXenes. In addition, the selectivity of MXene-based chemical sensors can be controlled by varying the interlayer charge transport of the MXenes (Koh et al., 2019).

3.1.3 Gas sensors

Gas sensors typically consist of a transducer and an active layer, which converts a reaction with the target gas into an electronic signal, such as a change in the resistance, capacitance, or frequency (Nazemi et al., 2019). The development of gas sensors with high sensitivity and rapid response has attracted significant research interest for various applications, including air pollution monitoring, food quality control, and biomedical applications (Jian et al., 2020). The emerging novel nanomaterials with inherent flexibility, as well as deposition techniques for the fabrication of flexible devices, have been utilized to develop flexible gas sensors (Alrammouz et al., 2018). Recently, the gas sensing properties of MXenes have also been investigated. Metallic MXenes always show a resistance increase under oxidizing or reducing gases because they have metallic conductivity, and gas adsorption reduces their charge carrier density. This is distinctive from other 2D semiconducting materials where the resistance can be increased or decreased depending on the gas molecules' electron-donating or accepting properties and the semiconducting material's type (p- or n-type) (Chen et al., 2020a). Surface terminations of MXenes have significant effects on the gas sensing properties of MXenes (Hajian et al., 2018). The gas sensing mechanism mainly depends on the electron transfer between gas molecules and the MXene (Huang et al., 2018). MXenes facilitate room-temperature gas sensing and are one of the appropriate candidates for the development of low-power and low-cost gas sensors (Liu et al., 2017). The key challenge in developing MXene-based gas sensors is aggregation, which can decrease their sensitivity and selectivity (Joshi et al., 2021). In addition to modifying the surface functional groups, the sensitivity and selectivity of MXene-based gas sensors can be controlled by modifying the interlayer spacing and transport of MXenes (Koh et al., 2019). Another solution for improving selective gas sensing is to use artificial intelligence methods for analyzing the data from gas sensor arrays (Li et al., 2021).

Kim et al. developed highly sensitive and low-noise MXene-based gas sensors with a very low limit of detection (LOD) for the detection of VOC gases at room temperature (Kim et al., 2018). The developed MXene-based gas sensors showed high selectivity toward hydrogen-bonding gases over acidic gases and the empirical LOD of 50 ppb. The signal-to-noise ratio of $Ti_3C_2T_x$-based sensors was two orders of magnitude higher than that of other 2D materials due to the high metallic conductivity of the $Ti_3C_2T_x$ for low noise and abundant

TABLE 3 Summary of MXene-based gas sensors.

Sensing material	Target gases	Limit of detection (ppb)	Sensitivity	Response/Recovery time (s)	Ref
3D MXene framework	Acetone, methanol, ethanol	50	0.10–0.17 %/ppm	90/102	Yuan et al. (2018)
Alkalized $Ti_3C_2T_x$ MXene	Ammonia	-	~0.29%/ppm	-	Yang Z. et al. (2019)
	Humidity	-	~ -1.19%/%RH	1/201	
$Ti_3C_2T_x$ MXene	Acetone, ethanol, ammonia, propanal	50–100	0.008–0.017 %/ppm	-	Kim et al. (2018)
$Ti_3C_2T_x$ MXene	Acetone, methanol, ethanol, ammonia	9,270	0.075–0.210 %/ppm	-	Lee et al. (2017)
V_2CT_x MXene	hydrogen, ethanol, acetone, methane, ammonia	1,375	0.005–0.2435 %/ppm	120/420 for hydrogen 480/330 for methane	Lee et al. (2019)
$W_{18}O_{49}/Ti_3C_2T_x$ MXene composite	Acetone	170	~ −4.57%/ppm	5.6/6	Sun et al. (2020)
$Ti_3C_2T_x$ MXene/WSe_2	Ethanol	-	−0.23%/ppm	9.7/6.6	Chen et al. (2020b)
SnO-$SnO_2/Ti_3C_2T_x$ MXene	Acetone	-	11.1%/ppm	18/9	Wang Z. J. et al., 2021
PVA/MXene	Humidity	-	−1.15%/%RH	0.9/6.3	Wang D. et al. (2021)
Berlin green/Ti_3CN MXene	Ammonia	-	-	88/142	Yang et al. (2021)

surface functional groups for a strong signal. It was revealed that the high sensitivity of $Ti_3C_2T_x$ MXene could be attributed to the strong interaction of surface functional groups with gas molecules and the excellent metallic conductivity of the core channels. Lee et al. developed a room-temperature NH_3 gas sensor based on $Ti_3C_2T_x$ MXene, showing the promising performance of the titanium carbide MXene as the NH_3 sensor (Lee et al., 2017). The sensing layer was formed by solution-casting of the synthesized $Ti_3C_2T_x$ suspension on platinum-based interdigitated electrodes (IDEs) sputtered on a flexible polyimide film. The developed sensor showed the capability to sense an array of VOC gases such as ethanol, methanol, acetone, and ammonia at room temperature, showing a higher sensing response to ammonia (Figure 9A). The gas sensing mechanism of $Ti_3C_2T_x$ involves the adsorption of gas molecules on defects and functional groups (Figure 9A). The $Ti_3C_2T_x$ MXene exhibited a p-type sensing behavior, possibly attributed to the adsorbed molecules such as water and oxygen introduced during the MXene synthesis process, which would play the role of a p-type dopant for $Ti_3C_2T_x$. The possible sensing mechanism of the sensor included electron transfer from adsorbed gas molecules to the $Ti_3C_2T_x$, which decreased the concentration of majority charge carriers (holes), resulting in a resistance increase in the MXene-based sensing layer. The possible electron transfer process between chemical species of the $Ti_3C_2T_x$ surface and NH_3 gas was proposed based on the following routes:

$$2NH_3 + 3O^- \rightarrow N_2 + 3H_2O + 3e^- \quad (1)$$

$$NH_3 + OH^- \rightarrow NH_2 + H_2O + e^- \quad (2)$$

The electrons generated through Eqs. 1, 2 leads to electron-hole recombination, followed by an increase of MXene film's electrical resistance. Recently, alkaline-treated $Ti_3C_2T_x$ MXenes have shown promising NH_3 and humidity sensing performance (Yuan et al., 2018). $Ti_3C_2T_x$ MXene was synthesized by the HF acid etching method, and alkalized $Ti_3C_2T_x$ was obtained by further alkaline-treating of MXenes with a sodium hydroxide (NaOH) solution. Room-temperature gas and humidity sensors were fabricated utilizing the dip-coating method. The fabricated sensors showed ~6,000% relative resistance change when the relative humidity (RH) varied from 11% to 95%. Also, the NH_3 sensing test at room temperature revealed a 28.87% relative resistance change in response to 100 ppm of NH_3. It was concluded that the intercalation of the alkali metal ion (Na^+) and the larger ratio of -O to -F surface functional groups in the MXene could significantly enhance humidity- and gas-sensing properties of the MXene at room temperature. In another work, a 3D MXene framework (3D-M) has been used to develop a room-temperature flexible VOC sensor, using the electrospinning technique and a self-assembly approach (Yang et al., 2019a). The interconnected porous structure of the fabricated sensor allows easy diffusion of gas molecules. The obtained sensors were tested for various VOCs (acetone, methanol, and ethanol) and showed a sensing range from 50 ppb up to saturated vapor, response and recovery time of less than 2 min, and no

performance decrease for 1,000 bending cycles. Recently, SnO-SnO_2/$Ti_3C_2T_x$ nanocomposites, developed by a one-step hydrothermal method, were used to develop acetone sensors (Wang Z. J. et al., 2021). The sensors exhibited a gas response value of 12.1, much higher than that of the pristine SnO-SnO_2 and $Ti_3C_2T_x$, and a recovery time of 9 s, under 100 ppm acetone at room temperature. It was suggested that the superior acetone sensitivity of the SnO-SnO_2/$Ti_3C_2T_x$ nanocomposite is attributed to its unique layered structure, larger specific surface area, and more extensive oxygen vacancies than $Ti_3C_2T_x$ gas sensors. Also, the p-n hetero-junction formation in the SnO-SnO_2/$Ti_3C_2T_x$ nanocomposite improves the response performance and reduces the induction temperature.

Density functional theory (DFT) calculations have been used to study the gas sensing properties of MXenes. As surface terminations play a significant role in the gas sensing of MXenes, optimizing the surface functional groups of MXenes is essential for improving the sensitivity of MXenes toward the target gas (Hajian et al., 2021). Khakbaz et al. used titanium carbide MXene models with different ratios of surface functional groups to represent MXene samples produced by different synthesis methods to study the impact of the synthesis method and surface terminations on the NH_3 sensing properties of MXenes (Figure 9B) (Khakbaz et al., 2019). It was demonstrated that $Ti_3C_2T_x$ MXenes with a low ratio of -F surface functional groups have a high NH_3 sensitivity, and the presence of water molecules in MXene samples can decrease the electron transfer between NH_3 molecule and the $Ti_3C_2T_x$ significantly. Yu et al. utilized DFT calculations to analyze the gas sensing behavior of monolayer oxygen-terminated titanium carbide MXene (Ti_2CO_2) (Yu et al., 2015). The Ti_2CO_2 MXene showed higher sensitivity to NH_3 when compared to other gases, including H_2, CH_4, CO, CO_2, N_2, NO_2, and O_2 molecules. Also, it was shown that the monolayer Ti_2CO_2 with biaxial strains larger than 3% could be used as an NH_3 capturer (Figure 9C), taking the adsorption energy of -0.50 eV as the reference for the gas capturer (Xiao et al., 2016). The NH_3 capture process is reversible, by releasing the applied strain. Xiao et al. investigated the effect of using different early transition metal elements for the adsorption of NH_3 on MXenes (Xiao et al., 2016). DFT calculations were employed to compare the sensing behavior of different oxygen-terminated M_2C MXenes (M = Sc, Ti, Zr, and Hf). It was shown that the impact of electron injection on the adsorption of NH_3 on Ti_2CO_2 is significantly more than those of other M_2CO_2 MXenes (M = Sc, Zr, and Hf), revealing that Ti_2CO_2 is the most sensitive M_2CO_2 MXene for NH_3 sensing (Figure 9D). Table 3 provides information about recently developed MXene-based gas sensors.

3.2.2 Electrochemical sensors

Electrochemical sensor is a device that converts the chemical information of a sample into an analytical signal. In a commonly used three-electrode electrochemical sensor, a potential is applied to the working electrode with respect to the reference electrode, while the counter electrode is used to complete the electrical circuit. In biosensors, bioreceptors such as enzymes, antibodies, and metal ions, are immobilized on electrodes for detection of target analytes and biomarkers, and techniques such as voltammetry and amperometry will be used to obtain the corresponding electrical signals which reflect the interaction between the bioreceptors and target analytes (Singh et al., 2016). Electrochemical sensors are utilized in various applications, such as the detection of heavy metal ions, glucose, and biomarkers of fatal diseases (Singh et al., 2016). Nanomaterials have received significant attention for the development of novel electrodes, which can improve electrochemical (bio) sensors' properties, such as sensitivity, selectivity, detection limits, and dynamic ranges. Recently, MXenes have also been used for the fabrication of electrochemical sensors and biosensors. In addition to great surface chemistry and high conductivity, the biocompatibility of MXenes is one of the key factors that makes it a highly promising choice for the fabrication of biosensors (Soleymaniha et al., 2019). However, there are concerns about biosafety because most synthesis methods of MXenes include using environmentally unfriendly HF, which can be addressed by developing environmentally friendly synthesis methods. Also, synthesizing new types of MXenes and controlling their surface functional groups can help to expand the electrochemical sensing applications of MXenes (Cheng et al., 2021).

Recently, an H_2O_2 sensor was fabricated by the deposition of a nanocomposite of titanium carbide MXene and Pt nanoparticles on the surface of a glassy carbon electrode (GCE) (Lorencova et al., 2018). The fabricated sensor exhibited a limit of detection (LOD) of 448 nM, while the reduction started at the potential of ~250 mV (vs Ag/AgCl). Moreover, the $Ti_3C_2T_x$/PtNP sensor was used to detect small redox molecules such as ascorbic acid (AA), dopamine (DA), uric acid (UA), and acetaminophen (APAP) at a potential higher than +250 mV, which showed high selectivity and low LOD (nM range). MXenes have been investigated for the development of wearable electrochemical biosensors for sweat analysis. A stretchable and wearable biosensor based on MXene/Prussian blue (Ti_3C_2/PB) composite has been fabricated for the detection of biomarkers (*e.g.*, glucose and lactate) in sweat (Figure 10A) (Lei et al., 2019). Experiments performed by utilizing artificial sweat showed electrochemical sensitivities of 35.3 μA mM^{-1} cm^{-2} for glucose and 11.4 μA mM^{-1} cm^{-2} for lactate. The wearable sweat-monitoring patch was used to detect the glucose and lactate levels during the *in-vitro* perspiration monitoring of human subjects, thereby exhibiting high sensitivity and good repeatability. In another work, Kumar et al. used MXene for the development of a biosensor for the detection of cancer biomarkers (carcinoembryonic antigen, CEA), utilizing aminosilane-functionalized Ti_3C_2 MXene for the covalent

TABLE 4 Summary of MXene-based electrochemical sensors.

Sensing material	Analyte	Detection method	Detection limit	Detection range	Ref
GOx/CNTs/$Ti_3C_2T_x$/PB/CFMs	Glucose	Chronoamperometry	0.33 μM	10 μM-1.5 mM	Lei et al. (2019)
LO/CNTs/$Ti_3C_2T_x$/PB/CFMs	Lactate	Chronoamperometry	0.67 μM	10 μM-22 mM	Lei et al. (2019)
BSA/Anti-CEA/f-Ti_3C_2/GCE	CEA	Cyclic voltammetry	18 fg/ml	100 fg/mL-2 μg/ml	Kumar et al. (2018)
Ta_2C	SARS-CoV-2 S protein	Surface-enhanced Raman spectroscopy	5 nM	-	Peng et al. (2021)
$Ti_3C_2T_x$	Carbendazim	Differential pulse voltammetry	10.3 nM	50 nM-100 μM	Wu D. H. et al. (2019)
MXene/GCE	H_2O_2	Chronoamperometry	0.7 nM	-	Lorencova et al. (2017)
MXene/PtNP/GCE	H_2O_2	Amperometry	448 nM	490 μM-53.6 mM	Lorencova et al. (2018)
MXene/PtNP/GCE	Ascorbic acid	Differential pulse voltammetry	0.25 μM	Up to 750 μM	Lorencova et al. (2018)
	Dopamine		0.26 μM		
	Uric acid		0.12 μM		
	Acetaminophen		0.13 μM		
AChE/Chit/MXene/AuNPs/MnO_2/Mn_3O_4/GCE	Methamidophos	Differential pulse voltammetry	0.134 p.m.	1 pM-1 μM	Song et al. (2019)
Urease/MB/MXene/SPE	Uric acid	Square wave voltammetry	5 μM	30–500 μM, 0.1–3.0 μM	Liu et al. (2019)
	Urea		0.02 μM		
MB/MXene/SPE	Creatinine	Square wave voltammetry	1.2 μM	10–400 μM	Liu et al. (2019)
$Ti_3C_2T_x$ MXene/ATP/$Mn_3(PO_4)_2$/GCE	Superoxide anion	Amperometry	0.5 nM	2.5 nM-14 μM	Zheng et al. (2019)
$Ti_3C_2T_x$/SPE	Acetaminophen	Differential pulse voltammetry	0.048 μM	0.25–2000 μM	Zhang Y. et al. (2019)
$Ti_3C_2T_x$/SPE	Isoniazid	Differential pulse voltammetry	0.064 μM	0.1–4.6 mM	Zhang Y. et al. (2019)
MXene/DNA/Pd/Pt/GCE	Dopamine	Amperometry	30 nM	0.2–1,000 μM	Zheng et al. (2018a)
MXene/GCE	BrO_3^-	Differential pulse voltammetry	41 nM	50 nM-5 μM	Rasheed et al. (2018)
Alkalized MXene/GCE	Cd^{2+}	Square wave anodic stripping voltammetry	98 nM	0.1–1.5 μM	Zhu X. et al. (2017)
	Pb^{2+}		41 nM		
	Cu^{2+}		32 nM		
	Hg^{2+}		130 nM		
GOx/Au/MXene/naf/GCE	Glucose	Amperometry	5.9 μM	0.1–18 mM	Rakhi et al. (2016)
Hb/naf/MXene/GCE	NO_2^-	Amperometry	0.12 μM	0.5 μM-11.8 mM	Liu et al. (2015)
Hb/naf/MXene/GCE	H_2O_2	Amperometry	0.02 μM	0.1–260 μM	Wang et al. (2015a)
TiO_2/Hb/naf/MXene/GCE	H_2O_2	Amperometry	14.0 nM	0.1–380 μM	Wang et al. (2015b)
Hb/MXene/GO/Au foil	H_2O_2	Differential pulse voltammetry	1.95 μM	2 μM-1 mM	Zheng et al. (2018b)
Tyr/MXene/chi/GCE	Phenol	Amperometry	12 nM	0.05–15.5 μM	Wu et al. (2018)
AchE/Chi/MXene/GCE	Malathion	Differential pulse voltammetry	3 fM	10 fM-10nM	Zhou et al. (2017)
MXene-FET	Dopamine	I_{ds}-V_{ds} characteristics	100 nM	0.1–50 μM	Xu et al. (2016)
MXene/GCPE	Adrenaline	Chronoamperometry	9.5 nM	0.02–10 μM	Shankar et al. (2018)
AChE/Ag/$Ti_3C_2T_x$/GCE	Malathion	Differential pulse voltammetry	3.27 fM	0.01 pM-0.01 μM	Jiang et al. (2018)
CRISPR-Cas12a/$Ti_3C_2T_x$-PEDOT:PSS/PDMS	HPV-related DNA	Current measurement	15.22 p.m.	0.02–50 nM	Zeng et al. (2021)

immobilization of anti-CEA. The fabricated bioelectrode (BSA/anti-CEA/f-Ti_3C_2-MXene/GC) showed a sensitivity of 37.9 μA ng^{-1} mL cm^{-2} per decade and a linear detection range of 0.0001–2000 ng ml^{-1} (Kumar et al., 2018). As the coronavirus disease 2019 outbreak has threatened human health globally, rapid and sensitive detection of SARS-CoV-2 viruses is of high importance. MXene has been used for the detection of SARS-CoV-2 S Protein (Peng et al., 2021). In this work, Nb_2C and Ta_2C MXenes exhibited a remarkable surface-enhanced Raman spectroscopy (SERS) enhancement, synergistically enabled by the charge transfer resonance and electromagnetic enhancement. The detection limit of Ta_2C MXene was 5×10^{-9} M, which helps real-time monitoring of novel coronavirus.

Song et al. used MnO_2/Mn_3O_4 and MXene/Au nanoparticles composites to develop a biosensor for the electrochemical detection of organophosphorus pesticides (OPs) (Song et al., 2019). Under optimum conditions, the developed sensor detected methamidophos in the concentration range of 10^{-12} M to 10^{-6} M, with good linearity (R^2 = 0.995), and a limit of detection of 1.34×10^{-13} M. In another work, dopamine (DA) sensors based on MXene/DNA/Pd/Pt nanocomposite were developed (Figure 10B) (Zheng et al., 2018a). The characterizations of the nanocomposite revealed that the DNA template plays a critical role in the formation of the nanocomposites. In the presence of DNA, the surface coverage ratio of MXene was increased, and the growth of PdNPs and Pd/Pt nanoparticles became more uniform in thickness. The fabricated sensor exhibited linear amperometric response in the DA concentration range of 0.2–1,000 μM, a detection limit of 30 nM, and high selectivity against ascorbic acid (AA), uric acid (UA), and glucose (Glu). Also, the fabricated sensors were used for the detection of DA in human serum samples. MXenes are also used for the detection of water contaminants. Recently, a sensor based on a lamellar $Ti_3C_2T_x$ MXene-modified glassy carbon electrode has been developed for the detection of bromate (BrO_3^-) in water (Rasheed et al., 2018). The developed sensor exhibited a linear response for the BrO_3^- concentration from 50 nM to 5 M, a detection limit of 41 nM, and high selectivity for BrO_3^-, among other interfering ions. Recently, Zeng et al. used a $Ti_3C_2T_x$-PEDOT:PSS/PDMS piezoresistive composite to develop a biosensor (Zeng et al., 2021). Clustered regularly interspaced short palindromic repeats (CRISPR) and corresponding effector proteins (Cas) were used to develop the CRISPR-Cas12a-mediated biosensor for point-of-care of human papillomavirus (HPV)-related DNA. The developed sensor exhibited good reproducibility, a LOD of ~15.22 p.m., and improved sensitivity compared to a traditional CRISPR-Cas12a fluorescence assay. Also, the signal readout from sensor devices and real-time wireless transmission were used to provide smartphone visual readout for remote monitoring of biomolecular signals. Table 4 includes some characteristics of MXene-based electrochemical sensors.

3.3 Optical sensors

An optical sensor is composed of a light source, a sensing platform for light-matter interactions, and a detector to quantify spectral shifts in electromagnetic waves resulting from the interaction with targeted analytes, which can be translated into quantitative or qualitative measurements (Law et al., 2020). Recently, MXenes have been used to develop high-performance optical sensors due to their unique properties: MXenes have a large specific surface area, excellent conductivity, wider absorption band, favorable energy levels, and possess hydrophilicity, excellent biocompatibility, and non-toxic to living organisms, which makes MXenes promising materials for developing optical sensors for biosensing applications (Zhu et al., 2021). MXenes have been used to develop different types of optical biosensors compatible with detection techniques, including surface plasmonic, fluorescent, electrochemiluminescence (ECL), and SERS (Bhardwaj et al., 2022). However, some gaps and challenges should be resolved to expand MXene's applications for optical sensing. MXenes have low quantum yields and photoluminescence in the UV region of the spectrum, which limits their applications in fluorescence and bio-imaging. Exploring more types of MXenes may help to resolve this problem and expand their applications in various optical sensing methods (Bhardwaj et al., 2022).

MXenes have been used for the fabrication of ultrasensitive surface plasmon resonance (SPR) biosensors for detecting carcinoembryonic antigen (CEA) (Figure 11A) (Wu Q. et al., 2019). The biosensor was developed on a Ti_3C_2-MXene-based sensing platform using multi-walled carbon nanotube (MWCNTs)-polydopamine (PDA)-Ag nanoparticle (AgNPs) signal enhancer It provided a dynamic range of 2×10^{-16} to 2×10^{-8} M and a detection limit of 0.07 fM for CEA detection. Also, the biosensor demonstrated good reproducibility and high specificity for CEA in real serum samples, providing a promising method for early diagnosis and monitoring of cancer. Wei et al. used MXene to develop a dual-mode ECL/SERS immunoassay for ultrasensitive determination of pathogenic bacteria, *Vibrio* vulnificus (VV) (Wei et al., 2021). The sensor was made with a multifunctional MXene material Rhodamine 6G (R6G)-$Ti_3C_2T_x$@ gold nanorods (AuNRs)-Ab2/ABEI which acts as an signal unit. The large surface area of MXene increased the number of signal tags and contributed to achieving a high detection sensitivity. The linear range of 1–10^8 CFU/ml and limit of quantification (LOQ) of 1 CFU/ml were measured for the ECL, and a linear range of 10^2–10^8 CFU/ml and LOQ of 10^2 CFU/ml were measured for the SERS. The sensors exhibited good stability, reproducibility, and selectivity and can potentially have broad applications in food safety and medical fields. Luo et al. used MXene quantum dots (QDs) to develop a biocompatibility nanoprobe for detecting intracellular Glutathione (GSH), where the N-Ti_3C_2 QDs acted as the

fluorescence reporters (Luo et al., 2021). The developed N-Ti_3C_2 QDs/Fe^{3+} nanoprobe displayed a high sensitivity, a detection limit of 0.17 μM, and a linear range of 0.5–100 μM for GSH. The developed probe looked promising in detecting and displaying cellular imaging of GSH in MCF-7 cells, and it might be used to establish a new imaging-guided precision cancer diagnosis method. MXene has also been used to develop an ultrasensitive ECL biosensor for exosomes and their surface proteins by *in-situ* formation of gold nanoparticles (AuNPs) decorated Ti_3C_2 MXenes hybrid with aptamer modification (AuNPs-MXenes-Apt) (Figure 11B) (Zhang et al., 2020).

The synergistic effects of large surface area, excellent conductivity, and catalytic effects of the AuNPs-MXenes-Apt led to the high sensitivity of the ECL biosensor towards exosome. The developed biosensors possessed a detection limit of 30 particles μL^{-1} for exosomes derived from HeLa cell line, the linear range of 10^2 to 10^5 particles μL^{-1}, and high selectivity toward exosomes and their surface proteins derived from different kinds of tumor cell lines (HeLa cells, OVCAR cells, and HepG2 cells). Wang et al. used MXenes to develop a label-free and visualized nanoplasmonic strategy for the detection of silver ions (Ag^+). In this work, o nly Ti_3C_2 MXenes were employed due to their excellent adsorption affinity and reductive property toward metal ions (Wang et al., 2020). Ag nanoparticles were capable of the colorimetric assay with a detection limit of 0.615 μM. RGB analysis exhibited visualized results consistent with the results measured on a UV–vis spectrometer, and the detection limits of Ag+ in real samples met the Drinking Water Standards set by the World Health Organization (WHO) and the United States Environmental Protection Agency (U.S. EPA). This sensor promises low-cost, simple-operation and on-site detection of metal ions.

4 Conclusion and outlook

Although MXenes were discovered just 11 years ago, these 2D materials have attracted significant research interest in a short time. Due to the promising physical and chemical properties of this material, MXenes have been used in various applications in healthcare, environment, and electronics for the development of various electronic devices, such as sensors, batteries, energy storage devices, nanogenerators, and antennas. MXenes are formulated as $M_{n+1}X_nT_x$, where M is an early transition metal (*e.g.*, Sc, Ti, V, Cr, Zr, Nb, Mo, Hf, Ta), X refers to C and/or N, T refers to surface functional groups (–OH, –O and–F), and n is an integer from 1 to 3. Since MXenes can contain different transition metals, various MXene materials with a range of physical and chemical properties can be synthesized. Also, the recently developed double transition metal MXenes have expanded the MXenes family.

In this review, the application of MXenes for the development of different sensor types has been summarized. MXenes are promising candidates for the development of sensors due to their interesting properties, such as high metallic conductivity, easy functionalization, high hydrophilicity, and good intercalation properties. MXenes have been used for the development of wearable sensors and electronic devices. Also, they can be integrated into textiles to develop fabric-based electronic devices and pressure sensors with high stability and sensitivity. The MXene-based pressure sensors can detect not just high pressure ranges but also low/weak pressures, which can be employed for gait monitoring applications. MXenes are also used to develop strain sensors with high stability, sensitivity, and stretchability. MXene-based room-temperature gas sensors can be used in healthcare diagnostics by detection of biomarkers and environmental applications by the detection of air pollutants or toxic gases. MXenes can also be used for the development of biosensors for detecting various biomarkers that can have applications in early diagnostic purposes/disease detection. Also, the reported MXene-based electrochemical sensors have exhibited low LODs. In addition, the high conductivity and large surface area of MXenes with various functional groups make them potential candidates for the development of electrochemical sensors for selective detection of various analytes. Also, the high biocompatibility of MXenes makes them a promising material for biomedical applications.

MXenes are promising materials for the development of functional inks and suspensions for application in flexible hybrid electronics (FHE). MXenes are hydrophilic and can be dispersed in water and polar solvents effectively, which can be related to the polar surface groups of MXenes. In addition to the high dispersion stability of MXene-based suspensions and inks, the synthesis of MXene-based nanocomposites can broaden the applications of MXenes in various technology areas. MXene-based nanocomposites with modified electrical, chemical, and physical properties can be used to improve the performance of MXene-based sensors and electronic devices. Also, the incorporation of interlayer spacers can modify the properties of the MXene-based sensors.

Although MXenes have already been used for the fabrication of various sensors and electronic devices, further research is needed to develop novel MXenes and improve the synthesis process, fabrication, and performance of MXene-based devices. Most of the MXene-based sensors contain titanium carbide MXene, so there is a need to investigate other MXenes to find the best choice for the mass-production of flexible sensors. Also, most MXenes have different surface functional groups, while the development of MXenes with a single type of surface termination group is desirable for controlling surface properties of the MXene, such as the affinity towards specific chemicals (selectivity). Further, DFT studies have shown that the synthesis of MXenes with no surface functional groups can change the chemical properties of MXenes significantly (Junkaew and Arróyave, 2018), which can be of high research interest for the development of chemical sensors. One of the concerns for the development of MXene-based

composites is the oxidation of MXenes in water, which needs more investigation to solve the problem. Specifically, water-based MXene suspensions can be used for the development of water-based inks that can be utilized for the fabrication of printed sensors and electronic devices using printed electronics techniques. Optimized MXene-based inks can be used for roll-to-roll mass-production of sensors, which reduces the final product cost and provides flexible sensors with a wide range of applications. Other challenges of the mass-production of MXene-based sensors include reducing the cost of MAX phases and improving the process of MXenes synthesis and modifications. Since HF-based synthesis methods are hazardous, safer methods are needed for the synthesis of MXenes. This review will help researchers by providing insight into the development of MXene-based physical and chemical sensors for a wide range of applications.

Author contributions

SH contributed to the design of the study, literature review, writing, and revising of the manuscript. DM, BN, and MA contributed to the literature review and revising the manuscript. All authors have read and approved the submitted version.

Conflict of interest

The authors declare that the research was conducted in the absence of any commercial or financial relationships that could be construed as a potential conflict of interest.

Publisher's note

All claims expressed in this article are solely those of the authors and do not necessarily represent those of their affiliated organizations, or those of the publisher, the editors and the reviewers. Any product that may be evaluated in this article, or claim that may be made by its manufacturer, is not guaranteed or endorsed by the publisher.

References

Alhabeb, M., Maleski, K., Anasori, B., Lelyukh, P., Sin, S., Gogotsi, Y., et al. (2017). Guidelines for synthesis and processing of two-dimensional titanium carbide ($Ti_3C_2T_x$ MXene). *Chem. Mat.* 29, 7633–7644. doi:10.1021/acs.chemmater.7b02847

Alhabeb, M., Maleski, K., Mathis, T. S., Sarycheva, A., Hatter, C. B., Uzun, S., et al. (2018). Selective etching of silicon from Ti3SiC2 (MAX) to obtain 2D titanium carbide (MXene). *Angew. Chem. Int. Ed.* 57, 5444–5448. doi:10.1002/anie.201802232

Alrammouz, R., Podlecki, J., Abboud, P., Sorli, B., and Habchi, R. (2018). A review on flexible gas sensors: From materials to devices. *Sensors Actuators A Phys.* 284, 209–231. doi:10.1016/j.sna.2018.10.036

Anasori, B., Lukatskaya, M. R., and Gogotsi, Y. (2017). 2D metal carbides and nitrides (MXenes) for energy storage. *Nat. Rev. Mat.* 2, 16098. doi:10.1038/natrevmats.2016.98

Anasori, B., Shi, C., Moon, E. J., Xie, Y., Voigt, C. A., Kent, P. R. C., et al. (2016). Control of electronic properties of 2D carbides (MXenes) by manipulating their transition metal layers. *Nanoscale Horiz.* 1, 227–234. doi:10.1039/C5NH00125K

Anasori, B., Xie, Y., Beidaghi, M., Lu, J., Hosler, B. C., Hultman, L., et al. (2015). Two-dimensional, ordered, double transition metals carbides (MXenes). *ACS Nano* 9, 9507–9516. doi:10.1021/acsnano.5b03591

Bhardwaj, S. K., Singh, H., Khatri, M., Kim, K.-H., and Bhardwaj, N. (2022). Advances in MXenes-based optical biosensors: A review. *Biosens. Bioelectron. X.* 202, 113995. doi:10.1016/j.bios.2022.113995

Cai, Y., Shen, J., Ge, G., Zhang, Y., Jin, W., Huang, W., et al. (2018). Stretchable $Ti_3C_2T_x$ MXene/carbon nanotube composite based strain sensor with ultrahigh sensitivity and tunable sensing range. *ACS Nano* 12, 56–62. doi:10.1021/acsnano.7b06251

Carey, M., and Barsoum, M. W. (2021). MXene polymer nanocomposites: A review. *Mater. Today Adv.* 9, 100120. doi:10.1016/j.mtadv.2020.100120

Chen, W. Y., Jiang, X., Lai, S. N., Peroulis, D., and Stanciu, L. (2020b). Nanohybrids of a MXene and transition metal dichalcogenide for selective detection of volatile organic compounds. *Nat. Commun.* 11, 1302. doi:10.1038/s41467-020-15092-4

Chen, W. Y., Lai, S. N., Yen, C. C., Jiang, X. F., Peroulis, D., and Stanciu, L. A. (2020a). Surface functionalization of $Ti_3C_2T_x$ MXene with highly reliable superhydrophobic protection for volatile organic compounds sensing. *ACS Nano* 14, 11490–11501. doi:10.1021/acsnano.0c03896

Chen, Z., Hu, Y., Zhuo, H., Liu, L., Jing, S., Zhong, L., et al. (2019). Compressible, elastic, and pressure-sensitive carbon aerogels derived from 2D titanium carbide nanosheets and bacterial cellulose for wearable sensors. *Chem. Mat.* 31, 3301–3312. doi:10.1021/acs.chemmater.9b00259

Cheng, J., Lu, G., and Wan, H. (2021). Lamellar MXene : A novel 2D nanomaterial for electrochemical sensors. *J. Appl. Electrochem.* 51, 1509–1522. doi:10.1007/s10800-021-01593-7

Choi, W., Choudhary, N., Han, G. H., Park, J., Akinwande, D., and Lee, Y. H. (2017). Recent development of two-dimensional transition metal dichalcogenides and their applications. *Mat. TodayKidlingt.* 20 (3), 116–130. doi:10.1016/j.mattod.2016.10.002

Duan, L., D'hooge, D. R., and Cardon, L. (2020). Recent progress on flexible and stretchable piezoresistive strain sensors: From design to application. *Prog. Mat. Sci.* 114, 100617. doi:10.1016/j.pmatsci.2019.100617

Firouzjaei, M. D., Karimiziarani, M., Moradkhani, H., Elliott, M., and Anasori, B. (2022). MXenes: The two-dimensional influencers. *Mater. Today Adv.* 13, 100202. doi:10.1016/j.mtadv.2021.100202

Ge, G., Huang, W., Shao, J., and Dong, X. (2018). Recent progress of flexible and wearable strain sensors for human-motion monitoring. *J. Semicond.* 39, 011012. doi:10.1088/1674-4926/39/1/011012

Ghidiu, M., Lukatskaya, M. R., Zhao, M. Q., Gogotsi, Y., and Barsoum, M. W. (2014). Conductive two-dimensional titanium carbide 'clay' with high volumetric capacitance. *Nature* 516, 78–81. doi:10.1038/nature13970

Guo, Y., Zhong, M., Fang, Z., Wan, P., and Yu, G. (2019). A wearable transient pressure sensor made with MXene nanosheets for sensitive broad-range human-machine interfacing. *Nano Lett.* 19 (2), 1143–1150. doi:10.1021/acs.nanolett.8b04514

Hajian, S., Khakbaz, P., Moshayedi, M., Maddipatla, D., Narakathu, B. B., Turkani, V. S., et al. (2018). *Impact of different ratios of fluorine, oxygen, and hydroxyl surface terminations on Ti_3C_2Tx MXene as ammonia sensor: A first-principles study*. New Delhi, India: IEEE Sensors Conference, 28–31. doi:10.1109/ICSENS.2018.8589699

Hajian, S., Tabatabaei, S. M., Narakathu, B. B., Maddipatla, D., Masihi, S., Panahi, M., et al. (2021). "Chlorine-terminated titanium carbide MXene as nitrogen oxide gas sensor: A first-principles study," in 2021 IEEE International Conference on Flexible and Printable Sensors and Systems (FLEPS) (Manchester, United Kingdom: IEEE), 1–4. doi:10.1109/FLEPS51544.2021.9469784

Halim, J., Kota, S., Lukatskaya, M. R., Naguib, M., Zhao, M.-Q., Moon, E. J., et al. (2016). Synthesis and characterization of 2D molybdenum carbide (MXene). *Adv. Funct. Mat.* 26, 3118–3127. doi:10.1002/adfm.201505328

Halim, J., Lukatskaya, M. R., Cook, K. M., Lu, J., Smith, C. R., Naslund, L. A., et al. (2014). Transparent conductive two-dimensional titanium carbide epitaxial thin films. *Chem. Mat.* 26, 2374–2381. doi:10.1021/cm500641a

Han, F., Luo, S. J., Xie, L. Y., Zhu, J. J., Wei, W., Chen, X., et al. (2019). Boosting the yield of MXene 2D sheets via a facile hydrothermal-assisted intercalation. *ACS Appl. Mat. Interfaces* 11, 8443–8452. doi:10.1021/acsami.8b22339

Hart, J. L., Hantanasirisakul, K., Lang, A. C., Anasori, B., Pinto, D., Pivak, Y., et al. (2019). Control of MXenes' electronic properties through termination and intercalation. *Nat. Commun.* 10 (1), 522. doi:10.1038/s41467-018-08169-8

Heacock, M., Kelly, C. B., Asante, K. A., Birnbaum, L. S., Bergman, A. L., Bruné, M.-N., et al. (2015). E-Waste and harm to vulnerable populations: A growing global problem. *Environ. Health Perspect.* 124 (5), 550–555. doi:10.1289/ehp.1509699

Hope, M. A., Forse, A. C., Griffith, K. J., Lukatskaya, M. R., Ghidiu, M., Gogotsi, Y., et al. (2016). NMR reveals the surface functionalisation of Ti3C2 MXene. *Phys. Chem. Chem. Phys.* 18, 5099–5102. doi:10.1039/C6CP00330C

Hu, S. J., Li, S. B., Xu, W. M., Zhang, J., Zhou, Y., and Cheng, Z. X. (2019). Rapid preparation, thermal stability and electromagnetic interference shielding properties of two-dimensional Ti3C2 MXene. *Ceram. Int.* 45 (16), 19902–19909. doi:10.1016/j.ceramint.2019.06.246

Huang, K., Li, C., Li, H., Ren, G., Wang, L., Wang, W., et al. (2020). Photocatalytic applications of two-dimensional Ti_3C_2 MXenes: A review. *ACS Appl. Nano Mat.* 3 (10), 9581–9603. doi:10.1021/acsanm.0c02481

Huang, K., Li, Z., Lin, J., Han, G., and Huang, P. (2018). Two-dimensional transition metal carbides and nitrides (MXenes) for biomedical applications. *Chem. Soc. Rev.* 47, 5109–5124. doi:10.1039/C7CS00838D

Jian, Y., Hu, W., Zhao, Z., Cheng, P., Haick, H., Yao, M., et al. (2020). Gas sensors based on chemi-resistive hybrid functional nanomaterials. *Nano-Micro Lett.* 12, 71. doi:10.1007/s40820-020-0407-5

Jiang, Y. J., Zhang, X. N., Pei, L. J., Yue, S., Ma, L., Zhou, L. Y., et al. (2018). Silver nanoparticles modified two-dimensional transition metal carbides as nanocarriers to fabricate acetycholinesterase-based electrochemical biosensor. *Chem. Eng. J.* 339, 547–556. doi:10.1016/j.cej.2018.01.111

Joshi, N., Braunger, M. L., Shimizu, F. M., Riul, A., Jr, and Oliveira, O. N. (2021). Insights into nano-heterostructured materials for gas sensing: A review. *Multifunct. Mat.* 4 (3), 032002. doi:10.1088/2399-7532/ac1732

Jun, B.-M., Kim, S., Heo, J., Park, C. M., Her, N., Jang, M., et al. (2018). Review of MXenes as new nanomaterials for energy storage/delivery, and selected environmental applications. *Nano Res.* 12, 471–487. doi:10.1007/s12274-018-2225-3

Junkaew, A., and Arróyave, R. (2018). Enhancement of the selectivity of MXenes (M2C, M = Ti, V, Nb, Mo) via oxygen-functionalization: Promising materials for gas-sensing and -separation. *Phys. Chem. Chem. Phys.* 20, 6073–6082. doi:10.1039/C7CP08622A

Kalambate, P. K., Gadhari, N. S., Li, X., Rao, Z., Navale, S. T., Shen, Y., et al. (2019). Recent advances in MXene-based electrochemical sensors and biosensors. *TrAC Trends Anal. Chem.* 120, 115643. doi:10.1016/j.trac.2019.115643

Khakbaz, P., Moshayedi, M., Hajian, S., Soleimani, M., Binu, B. N., Bradley, J. B., et al. (2019). Titanium carbide MXene as NH_3 sensor: Realistic first-principles study. *J. Phys. Chem. C* 123, 29794–29803. doi:10.1021/acs.jpcc.9b09823

Khan, R., and Andreescu, S. (2020). MXenes-based bioanalytical sensors: Design, characterization, and applications. *Sensors* 20, 5434. doi:10.3390/s20185434

Khazaei, M., Arai, M., Sasaki, T., Chung, C. Y., Venkataramanan, N. S., Estili, M., et al. (2013). Novel electronic and magnetic properties of two-dimensional transition metal carbides and nitrides. *Adv. Funct. Mat.* 23, 2185–2192. doi:10.1002/adfm.201202502

Khazaei, M., Ranjbar, A., Arai, M., Sasaki, T., and Yunoki, S. (2017). Electronic properties and applications of MXenes: A theoretical review. *J. Mat. Chem. C* 5, 2488–2503. doi:10.1039/C7TC00140A

Khazaei, M., Ranjbar, A., Liang, Y., and Yunoki, S. (2019). "Electronic properties of MXenes from *ab initio* calculations perspectives," in *2D metal carbides and nitrides (MXenes)* (Switzerland: Springer Nature), 255–289. Chapter 14. doi:10.1007/978-3-030-19026-2_14

Kim, H., Wang, Z., and Alshareef, H. N. (2019). MXetronics: Electronic and photonic applications of MXenes. *Nano Energy* 60, 179–197. doi:10.1016/j.nanoen.2019.03.020

Kim, S. J., Koh, H. J., Ren, C. E., Kwon, O., Maleski, K., Cho, S. Y., et al. (2018). Metallic $Ti_3C_2T_x$ MXene gas sensors with ultrahigh signal-to-noise ratio. *ACS Nano* 12, 986–993. doi:10.1021/acsnano.7b07460

Koh, H. J., Kim, S. J., Maleski, K., Cho, S. Y., Kim, Y. J., Ahn, C. W., et al. (2019). Enhanced selectivity of Mxene gas sensors through metal ion intercalation: *In situ* X-ray diffraction study. *ACS Sens.* 4, 1365–1372. doi:10.1021/acssensors.9b00310

Kumar, S., Lei, Y. J., Alshareef, N. H., Quevedo-Lopez, M. A., and Salama, K. N. (2018). Biofunctionalized two-dimensional Ti3C2 MXenes for ultrasensitive detection of cancer biomarker. *Biosens. Bioelectron. X.* 121, 243–249. doi:10.1016/j.bios.2018.08.076

Law, C. S., Marsal, L. F., and Santos, A. (2020). "9—electrochemically engineered nanoporous photonic crystal structures for optical sensing and biosensing," in *Handbook of nanomaterials in analytical chemistry*. Editor C. Hussain (Amsterdam, Netherlands: Elsevier), 201–226. doi:10.1016/B978-0-12-816699-4.00009-8

Lee, E., VahidMohammadi, A., Prorok, B. C., Yoon, Y. S., Beidaghi, M., and Kim, D. J. (2017). Room temperature gas sensing of two-dimensional titanium carbide (MXene). *ACS Appl. Mat. Interfaces* 9, 37184–37190. doi:10.1021/acsami.7b11055

Lee, E., Vahidmohammadi, A., Yoon, Y. S., Beidaghi, M., and Kim, D. J. (2019). Two-dimensional vanadium carbide MXene for gas sensors with ultrahigh sensitivity toward nonpolar gases. *ACS Sens.* 4, 1603–1611. doi:10.1021/acssensors.9b00303

Lei, Y. J., Zhao, W. L., Zhang, Y. Z., Jiang, Q., He, J. H., Baeumner, A. J., et al. (2019). A MXene-based wearable biosensor system for high-performance *in vitro* perspiration analysis. *Small* 15 (19), 1901190. doi:10.1002/smll.201901190

Li, D., Liu, G., Zhang, Q., Qu, M., Fu, Y. Q., Liu, Q., et al. (2021). Virtual sensor array based on MXene for selective detections of VOCs. *Sensors Actuators B Chem.* 331, 129414. doi:10.1016/j.snb.2020.129414

Li, M., Lu, J., Luo, K., Li, Y., Chang, K., Chen, K., et al. (2019). Element replacement approach by reaction with lewis acidic molten salts to synthesize nanolaminated MAX phases and MXenes. *J. Am. Chem. Soc.* 141, 4730–4737. doi:10.1021/jacs.9b00574

Li, T., Chen, L., Yang, X., Chen, X., Zhang, Z., Zhao, T., et al. (2019). A flexible pressure sensor based on an MXene-textile network structure. *J. Mat. Chem. C Mat.* 7 (4), 1022–1027. doi:10.1039/c8tc04893b

Li, X. P., Li, Y., Li, X., Song, D., Min, P., Hu, C., et al. (2019). Highly sensitive, reliable and flexible piezoresistive pressure sensors featuring polyurethane sponge coated with MXene sheets. *J. Colloid Interface Sci.* 542, 54–62. doi:10.1016/j.jcis.2019.01.123

Liao, H., Guo, X., Wan, P., and Yu, G. (2019). Conductive MXene nanocomposite Organohydrogel for flexible, healable, low-temperature tolerant strain sensors. *Adv. Funct. Mat.* 29, 1904507. doi:10.1002/adfm.201904507

Liu, H., Chen, X., Zheng, Y., Zhang, D., Zhao, Y., Wang, C., et al. (2021). Lightweight, superelastic, and hydrophobic polyimide nanofiber/MXene composite aerogel for wearable piezoresistive sensor and oil/water separation applications. *Adv. Funct. Mat.* 31, 2008006. doi:10.1002/adfm.202008006

Liu, H., Duan, C., Yang, C., Shen, W., Wang, F., and Zhu, Z. (2015). A novel nitrite biosensor based on the direct electrochemistry of hemoglobin immobilized on MXene-Ti3C2. *Sensors Actuators B Chem.* 218, 60–66. doi:10.1016/j.snb.2015.04.090

Liu, J., Jiang, X., Zhang, R., Zhang, Y., Wu, L., Lu, W., et al. (2019). MXene–enabled electrochemical microfluidic biosensor: Applications toward multicomponent continuous monitoring in whole blood. *Adv. Funct. Mat.* 29, 1807326. doi:10.1002/adfm.201807326

Liu, X., Ma, T., Pinna, N., and Zhang, J. (2017). Two-dimensional nanostructured materials for gas sensing. *Adv. Funct. Mat.* 27, 1702168. doi:10.1002/adfm.201702168

Lorencova, L., Bertok, T., Dosekova, E., Holazova, A., Paprckova, D., Vikartovska, A., et al. (2017). Electrochemical performance of Ti3C2Tx MXene in aqueous media: Towards ultrasensitive H2O2 sensing. *Electrochim. Acta* 235, 471–479. doi:10.1016/j.electacta.2017.03.073

Lorencova, L., Bertok, T., Filip, J., Jerigova, M., Velic, D., Kasak, P., et al. (2018). Highly stable Ti3C2Tx (MXene)/Pt nanoparticles-modified glassy carbon electrode for H2O2 and small molecules sensing applications. *Sensors Actuators B Chem.* 263, 360–368. doi:10.1016/j.snb.2018.02.124

Luo, W., Liu, H., Liu, X., Liu, L., and Zhao, W. (2021). Biocompatibility nanoprobe of MXene N-Ti3C2 quantum dot/Fe3+ for detection and fluorescence imaging of glutathione in living cells. *Colloids Surfaces B Biointerfaces* 201, 111631. doi:10.1016/j.colsurfb.2021.111631

Lv, G., Wang, J., Shi, Z., and Fan, L. (2018). Intercalation and delamination of two-dimensional MXene (Ti3C2Tx) and application in sodium-ion batteries. *Mat. Lett.* 219, 45–50. doi:10.1016/j.matlet.2018.02.016

Ma, Y., Liu, N., Li, L., Hu, X., Zou, Z., Wang, J., et al. (2017). A highly flexible and sensitive piezoresistive sensor based on MXene with greatly changed interlayer distances. *Nat. Commun.* 8, 1207. doi:10.1038/s41467-017-01136-9

Ma, Y., Yue, Y., Zhang, H., Cheng, F., Zhao, W., Rao, J., et al. (2018). 3D synergistical MXene/reduced graphene oxide aerogel for a piezoresistive sensor. *ACS Nano* 12, 3209–3216. doi:10.1021/acsnano.7b06909

Malaki, M., Maleki, A., and Varma, R. S. (2019). MXenes and ultrasonication. *J. Mat. Chem. A* 7, 10843–10857. doi:10.1039/c9ta01850f

Mashtalir, O., Lukatskaya, M. R., Zhao, M. Q., Barsoum, M. W., and Gogotsi, Y. (2015). Amine-Assisted delamination of Nb2C MXene for Li-ion energy storage devices. *Adv. Mat.* 27, 3501–3506. doi:10.1002/adma.201500604

Mashtalir, O., Naguib, M., Dyatkin, B., Gogotsi, Y., and Barsoum, M. W. (2013b). Kinetics of aluminum extraction from Ti3AlC2 in hydrofluoric acid. *Mat. Chem. Phys.* 139, 147–152. doi:10.1016/j.matchemphys.2013.01.008

Mashtalir, O., Naguib, M., Mochalin, V. N., Dall'Agnese, Y., Heon, M., Barsoum, M. W., et al. (2013a). Intercalation and delamination of layered carbides and carbonitrides. *Nat. Commun.* 4, 1716. doi:10.1038/ncomms2664

Mehdi Aghaei, S., Aasi, A., and Panchapakesan, B. (2021). Experimental and theoretical advances in MXene-based gas sensors. *ACS Omega* 6, 2450–2461. doi:10.1021/acsomega.0c05766

Naguib, M., Kurtoglu, M., Presser, V., Lu, J., Niu, J. J., Heon, M., et al. (2011). Two-dimensional nanocrystals produced by exfoliation of Ti_3AlC_2. *Adv. Mat.* 23, 4248–4253. doi:10.1002/adma.201102306

Naguib, M., Unocic, R. R., Armstrong, B. L., and Nanda, J. (2015). Largescale delamination of multi-layers transition metal carbides and carbonitrides "MXenes. *Dalton Trans.* 44, 9353–9358. doi:10.1039/C5DT01247C

Nazemi, H., Joseph, A., Park, J., and Emadi, A. (2019). Advanced Micro- and nano-gas sensor technology: A review. *Sensors* 19, 1285. doi:10.3390/s19061285

Ng, V. M. H., Huang, H., Zhou, K., Lee, P. S., Que, W., Xu, J. Z., et al. (2017). Recent progress in layered transition metal carbides and/or nitrides (MXenes) and their composites: Synthesis and applications. *J. Mat. Chem. A* 5, 3039–3068. doi:10.1039/C6TA06772G

Peng, Y. S., Lin, C. L., Long, L., Masaki, T., Tang, M., Yang, L., et al. (2021). Charge-transfer resonance and electromagnetic enhancement synergistically enabling MXenes with excellent SERS sensitivity for SARS-CoV-2 S protein detection. *Nano-Micro Lett.* 13, 52. doi:10.1007/s40820-020-00565-4

Pu, J. H., Zhao, X., Zha, X. J., Bai, L., Ke, K., Bao, R. Y., et al. (2019). Multilayer structured AgNW/WPU-MXene fiber strain sensors with ultrahigh sensitivity and a wide operating range for wearable monitoring and healthcare. *J. Mat. Chem. A Mat.* 7, 15913–15923. doi:10.1039/C9TA04352G

Rakhi, R., Nayuk, P., Xia, C., and Alshareef, H. N. (2016). Novel amperometric glucose biosensor based on MXene nanocomposite. *Sci. Rep.* 6, 36422. doi:10.1038/srep36422

Rasheed, P. A., Pandey, R. P., Rasool, K., and Mahmoud, K. A. (2018). Ultrasensitive electrocatalytic detection of bromate in drinking water based on Nafion/Ti3C2Tx (MXene) modified glassy carbon electrode. *Sensors Actuators B Chem.* 265, 652–659. doi:10.1016/j.snb.2018.03.103

Rasool, K., Pandey, R. P., Rasheed, P. A., Buczek, S., Gogotsi, Y., and Mahmoud, K. A. (2019). Water treatment and environmental remediation applications of two-dimensional metal carbides (MXenes). *Mat. TodayKidlingt.* 30, 80–102. doi:10.1016/j.mattod.2019.05.017

Seyedin, S., Uzun, S., Levitt, A., Anasori, B., Dion, G., Gogotsi, Y., et al. (2020). MXene composite and coaxial fibers with high stretchability and conductivity for wearable strain sensing textiles. *Adv. Funct. Mat.* 30, 1910504. doi:10.1002/adfm.201910504

Shankar, S. S., Shereema, R. M., and Rakhi, R. B. (2018). Electrochemical Determination of Adrenaline using MXene/Graphite composite paste electrodes. *ACS Appl. Mat. Interfaces* 10, 43343–43351. doi:10.1021/acsami.8b11741

Shi, X., Wang, H., Xie, X., Xue, Q., Zhang, J., Kang, S., et al. (2019). Bioinspired ultrasensitive and stretchable MXene-based strain sensor via nacre-mimetic microscale "brick-and-mortar" architecture. *ACS Nano* 13 (1), 649–659. doi:10.1021/acsnano.8b07805

Singh, P., Pandey, S. K., Singh, J., Srivastava, S., Sachan, S., and Singh, S. K. (2016). Biomedical perspective of electrochemical nanobiosensor. *Nanomicro. Lett.* 8, 193–203. doi:10.1007/s40820-015-0077-x

Sinha, A., Dhanjai, H., Zhao, Y., Huang, X., Lu, J., Chen Jain, R., et al. (2018). MXene: An emerging material for sensing and biosensing. *TrAC Trends Anal. Chem.* 105, 424–435. doi:10.1016/j.trac.2018.05.021

Soleymaniha, M., Shahbazi, M.-A., Rafieerad, A. R., Maleki, A., and Amiri, A. (2019). Promoting role of MXene nanosheets in biomedical sciences: Therapeutic and biosensing innovations. *Adv. Healthc. Mat.* 8, 1801137. doi:10.1002/adhm.201801137

Song, D., Jiang, X., Li, Y., Lu, X., Luan, S., Wang, Y., et al. (2019). Metal–organic frameworks–derived MnO2/Mn3O4 microcuboids with hierarchically ordered nanosheets and Ti3C2 MXene/AuNPs composites for electrochemical pesticide detection. *J. Hazard. Mat.* 373, 367–376. doi:10.1016/j.jhazmat.2019.03.083

Sun, S., Wang, M., Chang, X., Jiang, Y., Zhang, D., Wang, D., et al. (2020). W18O49/Ti3C2Tx Mxene nanocomposites for highly sensitive acetone gas sensor with low detection limit. *Sensors Actuators B Chem.* 304, 127274. doi:10.1016/j.snb.2019.127274

Urbankowski, P., Anasori, B., Makaryan, T., Er, D., Kota, S., Walsh, P. L., et al. (2016). Synthesis of two-dimensional titanium nitride Ti4N3 (MXene). *Nanoscale* 8, 11385–11391. doi:10.1039/C6NR02253G

Uzun, S., Seyedin, S., Stoltzfus, A. L., Levitt, A. S., Alhabeb, M., Anayee, M., et al. (2019). Knittable and washable multifunctional MXene-coated cellulose yarns. *Adv. Funct. Mat.* 29, 1905015. doi:10.1002/adfm.201905015

Wang, D., Zhang, D., Li, P., Yang, Z., Mi, Q., and Yu, L. (2021). Electrospinning of flexible poly(vinyl alcohol)/MXene nanofiber-based humidity sensor self-powered by monolayer molybdenum diselenide piezoelectric nanogenerator. *Nano-Micro Lett.* 13, 57. doi:10.1007/s40820-020-00580-5

Wang, F., Yang, C., Duan, C., Xiao, D., Tang, Y., and Zhu, J. (2015a). An organ-like titanium carbide material (MXene) with multilayer structure encapsulating hemoglobin for a mediator-free biosensor. *J. Electrochem. Soc.* 162, B16–B21. doi:10.1149/2.0371501jes

Wang, F., Yang, C. H., Duan, M., Tang, Y., and Zhu, J. F. (2015b). TiO2 nanoparticle modified organ-like Ti3C2 MXene nanocomposite encapsulating hemoglobin for a mediator-free biosensor with excellent performances. *Biosens. Bioelectron. X.* 74, 1022–1028. doi:10.1016/j.bios.2015.08.004

Wang, H., Peng, R., Hood, Z. D., Naguib, M., Adhikari, S. P., and Wu, Z. (2016). Titania composites with 2D transition metal carbides as photocatalysts for hydrogen production under visible-light irradiation. *ChemSusChem* 9, 1490–1497. doi:10.1002/cssc.201600165

Wang, K., Lou, Z., Wang, L., Zhao, L., Zhao, S., Wang, D., et al. (2019). Bioinspired interlocked structure-induced high deformability for two-dimensional titanium carbide (MXene)/natural microcapsule-based flexible pressure sensors. *ACS Nano* 13, 9139–9147. doi:10.1021/acsnano.9b03454

Wang, S., Shao, H., Liu, Y., Tang, C., Zhao, X., Ke, K., et al. (2021). Boosting piezoelectric response of PVDF-TrFE via MXene for self-powered linear pressure sensor. *Compos. Sci. Technol.* 202, 108600. doi:10.1016/j.compscitech.2020.108600

Wang, Y., Wang, S., Dong, N., Kang, W., Li, K., and Nie, Z. (2020). Titanium carbide MXenes mediated *in situ* reduction allows label-free and visualized nanoplasmonic sensing of silver ions. *Anal. Chem.* 92 (6), 4623–4629. doi:10.1021/acs.analchem.0c00164

Wang, Z. J., Wang, F., Hermawan, A., Asakura, Y., Hasegawa, T., Kumagai, H., et al. (2021). SnO-SnO2 modified two-dimensional MXene Ti3C2T for acetone gas sensor working at room temperature. *J. Mat. Sci. Technol.* 73, 128–138. doi:10.1016/j.jmst.2020.07.040

Wei, W., Lin, H., Hao, T., Su, X., Jiang, X., Wang, S., et al. (2021). Dual-mode ECL/SERS immunoassay for ultrasensitive determination of Vibrio vulnificus based on multifunctional MXene. *Sensors Actuators B Chem.* 332, 129525. doi:10.1016/j.snb.2021.129525

Wen, N., Zhang, L., Jiang, D., Li, B., Sun, C., Guo, Z., et al. (2020). Emerging flexible sensors based on nanomaterials: Recent status and applications. *J. Mat. Chem. A* 8, 25499–25527. doi:10.1039/D0TA09556G

Wu, D. H., Wu, M. Y., Yang, J. H., Zhang, H. W., Xie, K. F., Lin, C. T., et al. (2019). Delaminated Ti3C2Tx (MXene) for electrochemical carbendazim sensing. *Mat. Lett.* 236, 412–415. doi:10.1016/j.matlet.2018.10.150

Wu, L., Lu, X., Wu, Z. S., Dong, Y., Wang, X., Zheng, S., et al.Dhanjai (2018). 2D transition metal carbide MXene as a robust biosensing platform for enzyme immobilization and ultrasensitive detection of phenol. *Biosens. Bioelectron. X.* 107, 69–75. doi:10.1016/j.bios.2018.02.021

Wu, Q., Li, N., Wang, Y., Liu, Y., Xu, Y., Wei, S., et al. (2019). A 2D transition metal carbide MXene-based SPR biosensor for ultrasensitive carcinoembryonic antigen detection. *Biosens. Bioelectron. X.* 144, 111697. doi:10.1016/j.bios.2019.111697

Wu, Z., Wei, L., Tang, S., Xiong, Y., Qin, X., Luo, J., et al. (2021). Recent progress in $Ti_3C_2T_X$ MXene-based flexible pressure sensors. *ACS Nano* 15 (12), 18880–18894. doi:10.1021/acsnano.1c08239

Xiao, B., Li, Y. C., Yu, X. F., and Cheng, J. B. (2016). MXenes: Reusable materials for NH3 sensor or capturer by controlling the charge injection. *Sensors Actuators B Chem.* 235, 103–109. doi:10.1016/j.snb.2016.05.062

Xu, B. Z., Zhu, M. S., Zhang, W. C., Zhen, X., Pei, Z. X., Xue, Q., et al. (2016). Ultrathin MXene-micropattern-based field-effect transistor for probing neural activity. *Adv. Mat.* 28, 3333–3339. doi:10.1002/adma.201504657

Xu, M., Liang, T., Shi, M., and Xu, H. C. (2013). Graphene-like two-dimensional materials. *Chem. Rev.* 113 (5), 3766–3798. doi:10.1021/cr300263a

Xuan, J., Wang, Z., Chen, Y., Liang, D., Cheng, L., Yang, X., et al. (2016). Organic-base-Driven intercalation and delamination for the production of functionalized titanium carbide nanosheets with superior photothermal therapeutic performance. *Angew. Chem. Int. Ed.* 128, 14569–14574. doi:10.1002/anie.201606643

Yan, T., Wang, Z., and Pan, Z. J. (2018). Flexible strain sensors fabricated using carbon-based nanomaterials: A review. *Curr. Opin. Solid State Mat. Sci.* 22 (6), 213–228. doi:10.1016/j.cossms.2018.11.001

Yang, K., Yin, F. X., Xia, D., Peng, H. F., Yang, J. Z., and Yuan, W. J. (2019). A highly flexible and multifunctional strain sensor based on a network-structured MXene/polyurethane mat with ultra-high sensitivity and a broad sensing range. *Nanoscale* 11, 9949–9957. doi:10.1039/C9NR00488B

Yang, S., Zhang, P., Wang, F., Ricciardulli, A. G., Lohe, M. R., Blom, P. W. M., et al. (2018). Fluoride-free synthesis of two-dimensional titanium carbide (MXene) using A binary aqueous system. *Angew. Chem. Int. Ed. Engl.* 57, 15717–15721. doi:10.1002/ange.201809662

Yang, T., Gao, L., Wang, W., Kang, J., Zhao, G., Li, D., et al. (2021). Berlin green framework-based gas sensor for room-temperature and high-selectivity detection of ammonia. *Nano-Micro Lett.* 13 (1), 63. doi:10.1007/s40820-020-00586-z

Yang, Y., Cao, Z., He, P., Shi, L., Ding, G., Wang, R., et al. (2019a). Ti3C2Tx MXene-graphene composite films for wearable strain sensors featured with high sensitivity and large range of linear response. *Nano Energy* 66, 104134. doi:10.1016/j.nanoen.2019.104134

Yang, Y., Shi, L., Cao, Z., Wang, R., and Sun, J. (2019b). Strain sensors with a high sensitivity and a wide sensing range based on a $Ti_3C_2t_x$(MXene) nanoparticle–nanosheet hybrid network. *Adv. Funct. Mat.* 29, 1807882. doi:10.1002/adfm.201807882

Yang, Z., Liu, A., Wang, C., Liu, F., He, J., Li, S., et al. (2019). Improvement of gas and humidity sensing properties of organ-like MXene by alkaline treatment. *ACS Sens.* 4, 1261–1269. doi:10.1021/acssensors.9b00127

Yi, F., Ren, H., Shan, J., Sun, X., Wei, D., and Liu, Z. (2018). Wearable energy sources based on 2D materials. *Chem. Soc. Rev.* 47, 3152–3188. doi:10.1039/C7CS00849J

Yu, X. F., Li, Y. C., Cheng, J. B., Liu, Z. B., Li, Q. Z., Li, W. Z., et al. (2015). Monolayer Ti2CO2: A promising candidate for NH3 sensor or capturer with high sensitivity and selectivity. *ACS Appl. Mat. Interfaces* 7, 13707–13713. doi:10.1021/acsami.5b03737

Yuan, W., Yang, K., Peng, H., Li, F., and Yin, F. (2018). A flexible VOCs sensor based on a 3D Mxene framework with a high sensing performance. *J. Mat. Chem. A Mat.* 6, 18116–18124. doi:10.1039/C8TA06928J

Yue, Y., Liu, N., Liu, W., Li, M., Ma, Y., Luo, C., et al. (2018). 3D hybrid porous Mxene-sponge network and its application in piezoresistive sensor. *Nano Energy* 50, 79–87. doi:10.1016/j.nanoen.2018.05.020

Zang, Y., Zhang, F., Di, C.-a., and Zhu, D. (2015). Advances of flexible pressure sensors toward artificial intelligence and health care applications. *Mat. Horiz.* 2, 140–156. doi:10.1039/C4MH00147H

Zeng, R., Wang, W., Chen, M., Wan, Q., Wang, C., Knopp, D., et al. (2021). CRISPR-Cas12a-driven MXene-PEDOT:PSS piezoresistive wireless biosensor. *Nano Energy* 82, 105711. doi:10.1016/j.nanoen.2020.105711

Zeng, Y., and Wu, W. (2021). Synthesis of 2D $Ti_3C_2T_x$ MXene and MXene-based composites for flexible strain and pressure sensors. *Nanoscale Horiz.* 6, 893–906. doi:10.1039/D1NH00317H

Zhang, C., Anasori, B., Seral-Ascaso, A., Park, S., McEvoy, N., Shmeliov, A., et al. (2017). Transparent, flexible, and conductive 2D titanium carbide (MXene) films with high volumetric capacitance. *Adv. Mat.* 29, 1702678. doi:10.1002/adma.201702678

Zhang, H., Wang, Z., Wang, F., Zhang, Y., Wang, H., and Liu, Y. (2020). *In situ* formation of gold nanoparticles decorated Ti_3C_2 MXenes nanoprobe for highly sensitive electrogenerated chemiluminescence detection of exosomes and their surface proteins. *Anal. Chem.* 92, 5546–5553. doi:10.1021/acs.analchem.0c00469

Zhang, J., Wan, L., Gao, Y., Fang, X., Lu, T., Pan, L., et al. (2019). Highly stretchable and self-healable MXene/polyvinyl alcohol hydrogel electrode for wearable capacitive electronic skin. *Adv. Electron. Mat.* 5, 1900285. doi:10.1002/aelm.201900285

Zhang, Y.-Z., Lee, K. H., Anjum, D. H., Sougrat, R., Jiang, Q., Kim, H., et al. (2018). MXenes stretch hydrogel sensor performance to new limits. *Sci. Adv.* 4, eaat0098. doi:10.1126/sciadv.aat0098

Zhang, Y., Jiang, X., Zhang, J., Zhang, H., and Li, Y. (2019). Simultaneous voltammetric determination of acetaminophen and isoniazid using MXene modified screen-printed electrode. *Biosens. Bioelectron. X.* 130, 315–321. doi:10.1016/j.bios.2019.01.043

Zhao, Y., Ippolito, S., and Samorì, P. (2019). Functionalization of 2D materials with photosensitive molecules: From light-responsive hybrid systems to multifunctional devices. *Adv. Opt. Mat.* 7, 1900286. doi:10.1002/adom.201900286

Zheng, J., Diao, J., Jin, Y., Ding, A., Wang, B., Wu, L., et al. (2018b). An inkjet printed Ti3C2-GO electrode for the electrochemical sensing of hydrogen peroxide. *J. Electrochem. Soc.* 165, B227–B231. doi:10.1149/2.0051807jes

Zheng, J., Wang, B., Ding, A., Weng, B., and Chen, J. (2018a). Synthesis of MXene/DNA/Pd/Pt nanocomposite for sensitive detection of dopamine. *J. Electroanal. Chem. (Lausanne).* 816, 189–194. doi:10.1016/j.jelechem.2018.03.056

Zheng, J., Wang, B., Jin, Y., Weng, B., and Chen, J. (2019). Nanostructured MXene-based biomimetic enzymes for amperometric detection of superoxide anions from HepG2 cells. *Microchim. Acta* 186, 95. doi:10.1007/s00604-018-3220-9

Zhou, L., Zhang, X., Ma, L., Gao, J., and Jiang, Y. (2017). Acetylcholinesterase/chitosan-transition metal carbides nanocomposites based biosensor for the organophosphate pesticides detection. *Biochem. Eng. J.* 128, 243–249. doi:10.1016/j.bej.2017.10.008

Zhu, J., Ha, E., Zhao, G., Zhou, Y., Huang, D., Yue, G., et al. (2017). Recent advance in MXenes: A promising 2D material for catalysis, sensor and chemical adsorption. *Coord. Chem. Rev.* 352, 306–327. doi:10.1016/j.ccr.2017.09.012

Zhu, X., Liu, B., Hou, H., Huang, Z., Zeinu, K. M., Huang, L., et al. (2017). Alkaline intercalation of Ti3C2 MXene for simultaneous electrochemical detection of Cd(II), Pb(II), Cu(II) and Hg(II). *Electrochim. Acta* 248, 46–57. doi:10.1016/j.electacta.2017.07.084

Zhu, X., Zhang, Y., Liu, M., and Liu, Y. (2021). 2D titanium carbide MXenes as emerging optical biosensing platforms. *Biosens. Bioelectron. X.* 171, 112730. doi:10.1016/j.bios.2020.112730